

CERN-PH-EP-2014-065

Submitted to: EPJ C

**Measurement of the centrality and pseudorapidity dependence
of the integrated elliptic flow in lead-lead collisions at
 $\sqrt{s_{NN}} = 2.76$ TeV with the ATLAS detector**

The ATLAS Collaboration

Abstract

The integrated elliptic flow of charged particles produced in Pb+Pb collisions at $\sqrt{s_{NN}} = 2.76$ TeV has been measured with the ATLAS detector using data collected at the Large Hadron Collider. The anisotropy parameter, v_2 , was measured in the pseudorapidity range $|\eta| \leq 2.5$ with the event-plane method. In order to include tracks with very low transverse momentum p_T , thus reducing the uncertainty in v_2 integrated over p_T , a $1 \mu\text{b}^{-1}$ data sample recorded without a magnetic field in the tracking detectors is used. The centrality dependence of the integrated v_2 is compared to other measurements obtained with higher p_T thresholds. A weak pseudorapidity dependence of the integrated elliptic flow is observed for central collisions, and a small decrease when moving away from mid-rapidity is observed only in peripheral collisions. The integrated v_2 transformed to the rest frame of one of the colliding nuclei is compared to the lower-energy RHIC data.

Measurement of the centrality and pseudorapidity dependence of the integrated elliptic flow in lead-lead collisions at $\sqrt{s_{\text{NN}}} = 2.76$ TeV with the ATLAS detector

The ATLAS Collaboration

Received: date / Accepted: date

Abstract The integrated elliptic flow of charged particles produced in Pb+Pb collisions at $\sqrt{s_{\text{NN}}} = 2.76$ TeV has been measured with the ATLAS detector using data collected at the Large Hadron Collider. The anisotropy parameter, v_2 , was measured in the pseudorapidity range $|\eta| \leq 2.5$ with the event-plane method. In order to include tracks with very low transverse momentum p_{T} , thus reducing the uncertainty in v_2 integrated over p_{T} , a $1 \mu\text{b}^{-1}$ data sample recorded without a magnetic field in the tracking detectors is used. The centrality dependence of the integrated v_2 is compared to other measurements obtained with higher p_{T} thresholds. A weak pseudorapidity dependence of the integrated elliptic flow is observed for central collisions, and a small decrease when moving away from mid-rapidity is observed only in peripheral collisions. The integrated v_2 transformed to the rest frame of one of the colliding nuclei is compared to the lower-energy RHIC data.

1 Introduction

The anisotropy in the azimuthal angle distribution of particles produced in heavy-ion collisions has been studied extensively due to its sensitivity to the properties of the produced hadronic medium [1, 2]. The final-state anisotropy arises from the initial spatial asymmetry of the overlap zone in the collision of two nuclei with non-zero impact parameter. The initial spatial asymmetry induces asymmetric pressure gradients that are stronger in the direction of the reaction plane and, due to the collective expansion, lead to an azimuthally asymmetric distribution of the ejected particles. The final-state anisotropy is customarily characterized by the coefficients v_n of the Fourier decomposition of the azimuthal angle distribution of the emitted particles [3].

The second Fourier coefficient v_2 is related to the elliptical shape of the overlap region in non-central heavy-ion collisions, and the higher flow harmonics reflect fluctuations in the initial collision geometry [4]. The first observation of elliptic flow, quantified by measurements of v_2 , at RHIC [5–8] were found to be well described by predictions based on relativistic hydrodynamics [9–11], providing compelling evidence that the created matter is strongly coupled and behaves like an almost perfect, non-viscous, fluid. Later studies show small deviations from ideal hydrodynamics, described in terms of the ratio of shear viscosity to entropy density [12–15].

First results from Pb+Pb collisions at $\sqrt{s_{\text{NN}}} = 2.76$ TeV [16–21] from the Large Hadron Collider (LHC) showed no change in the transverse momentum, p_{T} , dependence of elliptic flow from that measured at the highest RHIC energy, while the elliptic flow integrated over p_{T} [16, 20] was found to increase by about 30% from the RHIC energy of $\sqrt{s_{\text{NN}}} = 200$ GeV to $\sqrt{s_{\text{NN}}} = 2.76$ TeV at the LHC. This increase in the integrated elliptic flow with energy is therefore driven mostly by the increase in the mean p_{T} of the produced particles. The dependence of elliptic flow on the geometry of the collision (the collision centrality) is of particular importance, since the flow is thought to depend strongly on the initial spatial anisotropy. Hydrodynamical models are used to quantitatively relate the initial geometry to the experimentally measured distributions. Furthermore, recent hydrodynamical calculations [22, 23] also include a longitudinal dependence in the source shape, which can be deduced from flow measurements over a wide pseudorapidity range.

This article presents measurements of the centrality and pseudorapidity dependence of the elliptic flow integrated over the p_{T} of charged particles produced in Pb+Pb collisions at $\sqrt{s_{\text{NN}}} = 2.76$ TeV recorded in 2010 by the ATLAS detector.

In order to reduce the uncertainty in the p_T -integrated coefficient v_2 by including tracks with p_T lower than in the measurements reported by the ALICE [16] and CMS [20] experiments, a special track reconstruction procedure was applied to “field-off” data taken without the solenoid’s magnetic field in the tracking detectors. Other track reconstruction methods, applicable at higher p_T , were exploited in cross-checks using “field-on” data taken with the solenoid’s magnetic field.

2 The ATLAS detector

The ATLAS detector is a multi-purpose particle physics apparatus and is described in detail elsewhere [24]. This analysis uses the three-level trigger system to select Pb+Pb collision events, the forward calorimeters (FCal) to measure the collision centrality, and the inner detector (ID) to measure charged-particle tracks. The ID tracking system comprises silicon pixel and microstrip detectors and a transition radiation tracker. It provides complete azimuthal coverage and spans the pseudorapidity region $|\eta| < 2.5$.¹ The pixel detector consists of a three-layer barrel section and three discs in each of the forward regions. The semiconductor tracker has four double layers of microstrip sensors in its barrel section and nine discs in each of the forward regions. The ID is surrounded by a thin superconducting solenoid, which produces a 2 T axial magnetic field for the field-on data. The FCal measures both electromagnetic and hadronic energy, using copper–tungsten/liquid-argon technology, and provides complete azimuthal coverage for $3.2 < |\eta| < 4.9$. The hardware-based Level-1 trigger selected minimum-bias Pb+Pb collisions by requiring either a coincidence of signals recorded in the zero-degree calorimeters (ZDC) located symmetrically at $z = \pm 140$ m ($|\eta| > 8.3$) or a signal in at least one side of the minimum-bias trigger scintillators (MBTS) at $z = \pm 3.6$ m ($2.1 < |\eta| < 3.9$). To suppress beam backgrounds, the Level-2 trigger demanded MBTS signals from opposite sides of the interaction region and imposed a timing requirement on them.

With these trigger conditions, ATLAS recorded a sample of Pb+Pb collisions corresponding to an integrated luminosity of approximately $1 \mu\text{b}^{-1}$ taken with the field provided by the solenoid turned off. In addition, approximately $0.5 \mu\text{b}^{-1}$ of field-on data was used in studies of track reconstruction performance.

¹ ATLAS uses a right-handed coordinate system with its origin at the nominal interaction point (IP) in the centre of the detector and the z -axis along the beam pipe. The x -axis points from the IP to the centre of the LHC ring, and the y -axis points upward. Cylindrical coordinates (r, ϕ) are used in the transverse plane, ϕ being the azimuthal angle around the beam pipe. The pseudorapidity is defined in terms of the polar angle θ as $\eta = -\ln \tan(\theta/2)$.

3 Event selection and centrality definition

The offline event selection required each event to have a vertex formed by at least three charged-particle tracks reconstructed in the ID. The data were recorded at low instantaneous luminosity where the probability of multiple collisions per bunch crossing (pile-up) was negligible. The track reconstruction algorithms therefore allowed only one collision vertex (called the primary vertex) in each event, thereby reducing the processing time while maintaining efficiency. The time difference between the MBTS signals from the opposite sides of the interaction region was required to be less than 3 ns, and a coincidence of ZDC signals was also required. These additional selection criteria efficiently remove beam-gas and photo-nuclear interactions. As shown in previous studies [18], the applied trigger and offline requirements provide a minimum-bias event sample in which the fraction of inelastic Pb+Pb collisions is $98 \pm 2\%$.

Events satisfying the above criteria were also required to have a primary vertex within 50 mm (100 mm) in the z -direction of the nominal centre of the ATLAS detector for the field-off (field-on) data subsample. After requiring all relevant subdetectors to be performing normally, the subsamples used in the analysis of the field-off and field-on data contained approximately 1.6 million and 3 million minimum-bias events, respectively.

Monte Carlo (MC) event samples were used to determine the tracking efficiencies and the rates of fake tracks. The HIJING event generator [25] was used to produce minimum-bias Pb+Pb collisions. Events were generated with the default parameters except for jet quenching, which was turned off. The effect of elliptic flow was implemented after event generation. The azimuthal angles of final-state particles were redistributed at generator level to produce an elliptic flow consistent with previous ATLAS measurements [18, 19]. The simulation of the ATLAS detector’s response [26] to the generated events is based on the GEANT4 package [27] and included a detailed description of the detector geometry and material in the 2010 Pb+Pb run. Two samples of 0.5 million MC events were simulated, one with the solenoid field switched off and the other with it switched on. Additional MC samples consisting of 50,000 events simulated with 10–20% extra detector material were used to study systematic uncertainties. The generated charged particles were reweighted with p_T - and centrality-dependent functions so that the p_T spectra in the MC samples matched the experimental ones [28].

The centrality of the Pb+Pb collisions was characterized by the summed transverse energy, ΣE_T^{FCal} , measured in the FCal [18]. The ΣE_T^{FCal} distribution was divided into ten centrality bins, each representing 10% of the full distribution after accounting for 2% inefficiency in recording the most peripheral collisions (the 0–10% centrality interval corre-

sponds to the most central 10% of collisions: those with the largest $\Sigma E_{\text{T}}^{\text{FCal}}$). A small change in the overall recording efficiency leads to large fluctuations in the population of the most peripheral collisions. To avoid resulting large systematic uncertainties, the 20% of events with the smallest $\Sigma E_{\text{T}}^{\text{FCal}}$ were not included in the analysis.

4 Elliptic-flow measurement

The final-state azimuthal anisotropy is quantified by the coefficients in the Fourier expansion of the ϕ distribution of charged particles [3],

$$dN/d\phi \propto 1 + 2 \sum_{n=1}^{\infty} v_n \cos(n[\phi - \Psi_n]), \quad (1)$$

where v_n and Ψ_n are the magnitude and the azimuthal direction (called the event-plane angle) of the n -th flow harmonic, respectively.

The second flow harmonic, v_2 , for a given collision centrality is a function of p_{T} and η , and is determined by

$$v_2(\eta, p_{\text{T}}) = \frac{\langle \cos(2[\phi - \Psi_2]) \rangle}{\sqrt{\langle \cos(2[\Psi_2^{\text{N}} - \Psi_2^{\text{P}}]) \rangle}}, \quad (2)$$

where the numerator denotes the average over charged-particle tracks in a given η and p_{T} range, and the denominator, averaged over events, is a correction accounting for the finite experimental resolution in the determination of the event-plane angle Ψ_2 . This resolution correction was obtained using the sub-event technique [3] as described in Refs [18, 19]. The two ‘‘sub-events’’ defined for each event cover two η ranges of the same width in the positive and negative η hemispheres ($3.2 < |\eta| < 4.8$) of the FCal detector. The sub-event-plane angles are determined by

$$\Psi_2^{\text{N(P)}} = \frac{1}{2} \tan^{-1} \left(\frac{\sum_i E_{\text{T}i}^{\text{tower}} w_i \sin(2\phi_i)}{\sum_i E_{\text{T}i}^{\text{tower}} w_i \cos(2\phi_i)} \right), \quad (3)$$

where the sums run over transverse energies, $E_{\text{T}}^{\text{tower}}$, as measured in calorimeter towers located at negative (N) and positive (P) η in the first sampling layer of the FCal. The FCal towers consist of cells grouped into projective regions in $\Delta\eta \times \Delta\phi$ of 0.1×0.1 . The weights, $w_i = w_i(\phi_i, \eta_i)$, were determined in narrow $\Delta\eta$ slices ($\Delta\eta = 0.1$) over the full η range in order to remove structures in the uncorrected ϕ distributions of $E_{\text{T}}^{\text{tower}}$ in every $\Delta\eta$ slice and to ensure a uniform Ψ_2 distribution.

In the sub-event approach, potential non-flow correlations are minimized by using the reaction plane estimated from the η side opposite to the tracks used for the v_2 measurement; this provides a separation of $\Delta\eta > 3.2$. This method was previously applied [18] to measure v_2 as a function of p_{T} using charged-particle tracks reconstructed in the ID tracking system with a minimum p_{T} of 0.5 GeV.

In order to perform the integration over p_{T} , the differential v_2 measurements are weighted by the number of charged-particle tracks $N_{i,k}^{\text{corr}}$,

$$v_2 = \sum_i \sum_k v_2(\eta_i, p_{\text{T},k}) N_{i,k}^{\text{corr}} / \sum_i \sum_k N_{i,k}^{\text{corr}}, \quad (4)$$

and summed over bins in η (denoted by the index i) and p_{T} (index k). The number of charged-particle tracks is calculated as $N_{i,k}^{\text{corr}} = N_{i,k}[1 - f(i,k)]/\epsilon(i,k)$, where the $N_{i,k}$ is the observed number of tracks in a given η and p_{T} bin, $\epsilon(i,k)$ is the track reconstruction efficiency and $f(i,k)$ is the estimated rate of fake tracks. In the following sections, the lower limit in the integration of v_2 over p_{T} is denoted by $p_{\text{T},0}$.

5 Track reconstruction

The ID was used to reconstruct charged-particle trajectories. Three track reconstruction methods were applied in order to exploit a large range in particle p_{T} :

- the tracklet (TKT) method used for the field-off data in order to reach charged-particle p_{T} below 0.1 GeV [28],
- the pixel track (PXT) method used to reconstruct tracks with $p_{\text{T}} \geq 0.1$ GeV using only the pixel detector in the field-on data sample,
- the ID track (IDT) method for the field-on data sample, the default ATLAS reconstruction method, for which all ID sub-detectors are used and the track p_{T} is limited to $p_{\text{T}} \geq 0.5$ GeV [29].

In the TKT method for field-off data, tracks are formed from the positions of hit clusters in the inner two layers of the pixel detector and the position of the primary vertex reconstructed using ID tracks. In the first step, the η_0 and ϕ_0 coordinates are defined using the event’s vertex position and the hit recorded in the first pixel layer. Then a search for a hit in the second pixel layer (with η_1 and ϕ_1 coordinates defined with respect to the vertex position) is performed and its consistency with a straight-track hypothesis is checked. Candidate tracklets are required to satisfy the condition

$$\Delta R = \frac{1}{\sqrt{2}} \sqrt{\left(\frac{\Delta\eta}{\sigma_{\eta}(\eta_0)} \right)^2 + \left(\frac{\Delta\phi}{\sigma_{\phi}(\eta_0)} \right)^2} < N_{\sigma}, \quad (5)$$

where $\Delta\eta = \eta_1 - \eta_0$ and $\Delta\phi = \phi_1 - \phi_0$, and $\sigma_{\eta}(\eta_0)$ and $\sigma_{\phi}(\eta_0)$ are pseudorapidity-dependent widths of the $\Delta\eta$ and $\Delta\phi$ distributions, respectively. In this analysis, $N_{\sigma} = 3$ was used as the default condition. Clusters located close to each other in the second pixel layer are most likely to originate from the same particle. Therefore, if more than one cluster located in the second pixel layer fulfils the selection criteria, the resulting tracklets are merged into a single tracklet. The $\Delta\eta$ and $\Delta\phi$ distributions in data and MC simulation are compared in Fig. 1. The data and MC distributions agree

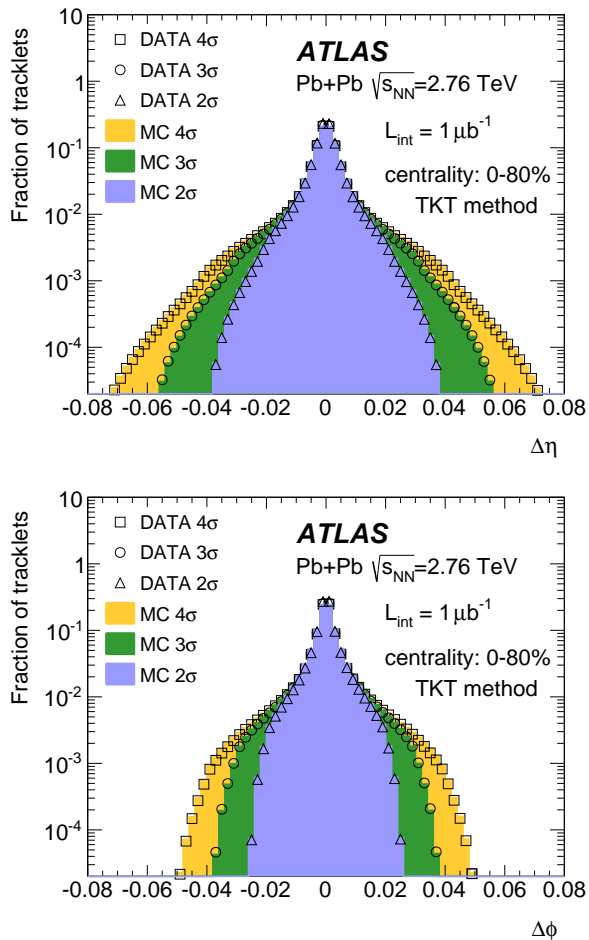


Fig. 1 Comparison of the tracklets' $\Delta\eta$ (top) and $\Delta\phi$ (bottom) distributions in data (open symbols) and MC simulation (filled histograms) for tracklets measured within the pseudorapidity range $|\eta| < 2$, for events in the 0–80% centrality interval and $\Delta R < 4\sigma, 3\sigma$ and 2σ (see Sect. 5 for details) as described in the legend.

well. Candidates fulfilling the criterion in Eq. (5) were accepted for further analysis with $\eta = \eta_0$ and $\phi = \phi_0$.

This method does not provide information about the track's p_T ; nevertheless, its performance can be checked as a function of generator-level particle p_T by applying the same reconstruction procedure to the MC simulation and using the p_T of the generated particle corresponding to the reconstructed tracklet whenever applicable. Figure 2 compares the p_T spectra of stable charged particles at the MC-generator level, N_{primary} , to the spectra of reconstructed tracklets matched to charged particles, N_{matched} , for three representative centrality bins and for $|\eta| < 1$. A particle was considered to be primary if it originated directly from the collision or resulted from the decay of a particle with $c\tau < 1$ mm. The matching criterion required that the two hits forming the tracklet be identical to the hits associated with a charged particle. The distributions show that the TKT

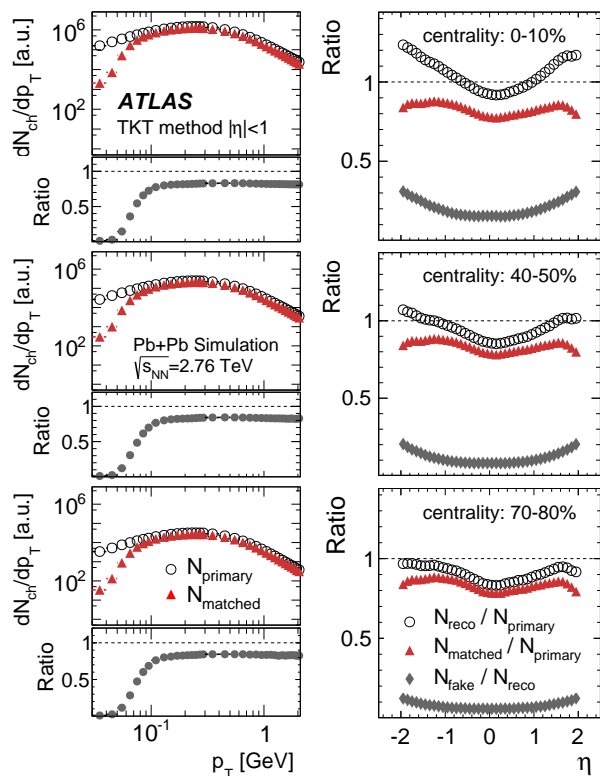


Fig. 2 Monte Carlo evaluation of the tracklet reconstruction performance in representative centrality bins 0–10%, 40–50% and 70–80%. Left: generator-level transverse momentum distributions of primary charged particles, N_{primary} (open circles), compared to the p_T spectra of charged particles matched to the reconstructed tracklets, N_{matched} (red triangles). Bottom panels show the ratios of the two distributions. Right: pseudorapidity, η , dependence of the ratio of all reconstructed tracklets, N_{reco} (open circles), and N_{matched} (red triangles) to all primary charged particles. The ratio of fake tracklets, N_{fake} (grey diamonds), to all reconstructed tracklets is also shown.

method is able to reconstruct particles with transverse momenta ~ 0.07 GeV with 50% efficiency, and that a plateau at about 80% is reached for $p_T > 0.1$ GeV in all centrality bins. For low p_T , the efficiency decreases sharply, but the particle density is small in this region, as is v_2 ; thus the contribution from this region to the integrated elliptic flow is expected to be small. Figure 2 also shows the reconstruction efficiency, $N_{\text{matched}}/N_{\text{primary}}$, as a function of η . Here, N_{primary} denotes all primary charged particles with $p_T \geq 0.07$ GeV, which defines the low- p_T limit for integrating v_2 over p_T . The efficiency is found to be $\sim 80\%$ and depends weakly on η . The rate of fake tracklets, N_{fake} , measured as the ratio of the number of tracklets not matched to charged particles to the total number of reconstructed tracklets, $N_{\text{fake}}/N_{\text{reco}}$, increases with centrality and $|\eta|$, reaching about 35% for the most central collisions at $|\eta| = 2$.

For field-on data, the PXT method allows the transverse momentum range $p_T > 0.1$ GeV to be examined. Tracks

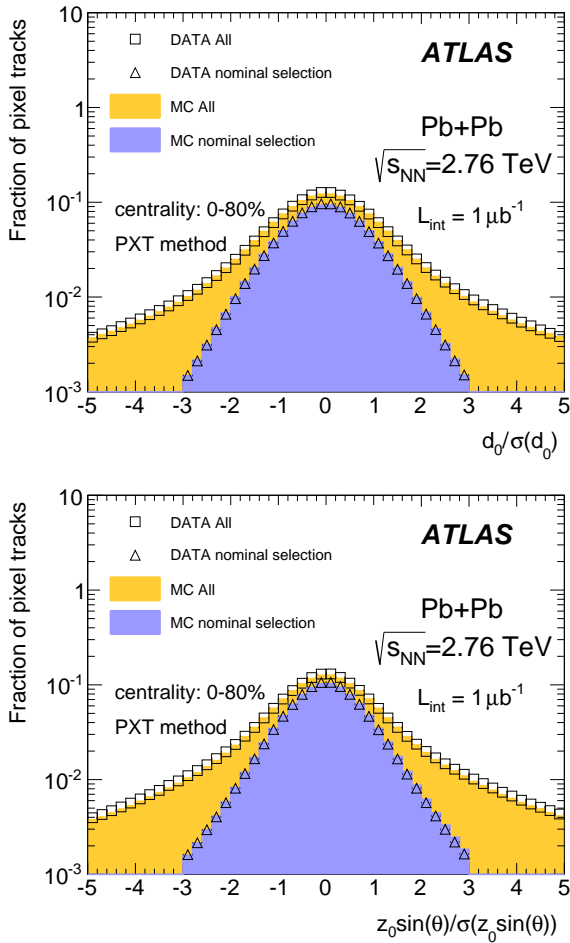


Fig. 3 Comparison of distributions of the transverse (top), and longitudinal (bottom) impact parameter significances in data and MC simulation for all reconstructed tracks and for the selected tracks (see text for details).

were reconstructed within the full acceptance of the pixel detector ($|\eta| < 2.5$). To improve the track reconstruction's performance in the heavy-ion collision environment, the track-quality requirements were made more stringent than those for proton–proton collisions [30]. Pixel tracks were required to have no missing hits in the pixel layers, and the transverse and longitudinal impact parameters, d_0 and z_0 , with respect to the vertex were required to have $|d_0|$ and $|z_0 \sin(\theta)|$ less than 1 mm and significances $|d_0/\sigma_{d_0}|$ and $|z_0 \sin \theta/\sigma_{z_0 \sin \theta}|$ less than 3.0. Figure 3 shows good agreement between data and MC simulation in the distributions of $|d_0/\sigma_{d_0}|$ and $|z_0 \sin \theta/\sigma_{z_0 \sin \theta}|$.

The pixel track method's reconstruction efficiency was evaluated in MC simulation by matching reconstructed tracks to the generated charged particles. A track is matched to a generated charged particle if it is reconstructed from at least 69% of the pixel hits originating from the latter. Figure 4 illustrates the dependence of the pixel track reconstruction efficiency on p_T in three pseudorapidity ranges

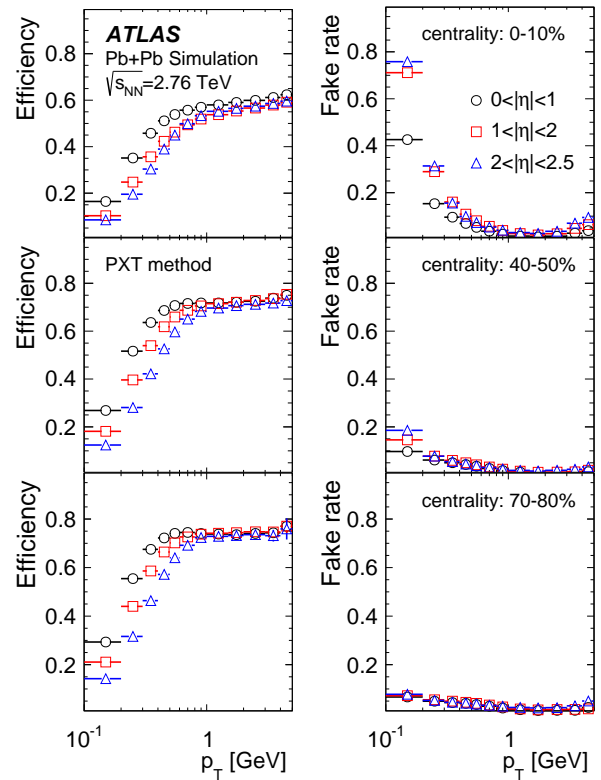


Fig. 4 The transverse momentum, p_T , dependence of the pixel track reconstruction efficiency (left) and the fake rate (right) for three pseudorapidity ranges and three centrality intervals as indicated in the legend.

and for three selected centrality bins. The efficiency decreases slightly from peripheral to central collisions and also deteriorates when moving away from mid-rapidity. A weak p_T dependence is observed above $p_T > 0.5$ GeV for all collision centralities. At lower p_T , the efficiency decreases with decreasing p_T and to about 20% at the lowest accessible p_T .

The fraction of fake tracks, defined as the ratio of reconstructed tracks not matched to generated charged particles to all reconstructed pixel tracks, was evaluated using MC simulation. Figure 4 shows the fake-rate dependence on p_T in three pseudorapidity ranges and for three centrality bins. The fake rate is below 10% for p_T above 0.4 GeV and depends very weakly on p_T and η for peripheral collisions. In more central collisions, the fake rate increases at low p_T and shows a similar increase with increasing $|\eta|$.

The performance of the PXT reconstruction method can be compared with that of the IDT method. The track reconstruction efficiency and rate of fake tracks from the IDT method are shown in Fig. 5 (for reconstruction details see Ref. [18]). The minimum p_T reached is 0.5 GeV. A comparison of Figs 4 and 5 shows that the extension towards lower p_T values for the PXT method is achieved at the expense of

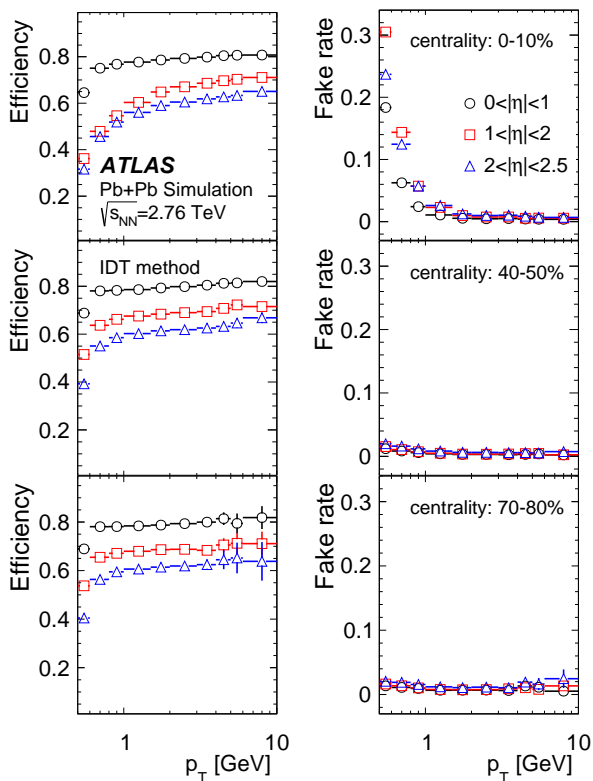


Fig. 5 The transverse momentum, p_T , dependence of the ID track reconstruction efficiency (left) and the fake rate (right) for three pseudorapidity ranges and three centrality intervals as indicated in the legend.

much larger fake rates than observed for the IDT method, whereas the reconstruction efficiencies are similar. The two methods have different p_T resolutions: it is very good for ID tracks, the root mean square of $(p_T^{\text{reco}}/p_T^{\text{true}} - 1)$ being, in $|\eta| < 1$, about 4% and independent of the track p_T in the used range, whereas for pixel tracks it is about 10% at the lowest p_T and increases to about 15% at 5 GeV.

The performance of the MC simulation in describing the fake rates in the data was checked by comparing the $\Delta\eta$, $\Delta\phi$, d_0/σ_{d_0} and $z_0 \sin\theta/\sigma_{z_0 \sin\theta}$ distributions, like the ones shown in Figs 1 and 3. Additionally, the distributions of the ratios of the number of tracklets and pixel tracks to the number of ID tracks in data and MC simulation were compared, as shown in Fig. 6. It can be concluded that the MC description of the TKT and PXT methods' performance is adequate.

The elliptic flow depends on the particle type [31], as does the reconstruction efficiency. Although the track reconstruction efficiency is averaged over all particle types in this analysis, the reconstruction efficiencies for simulated pions, kaons and protons are shown as a function of p_T in the Appendix. This information is important for comparison of measurements with theory predictions in which the elliptic flow depends on the particle type.

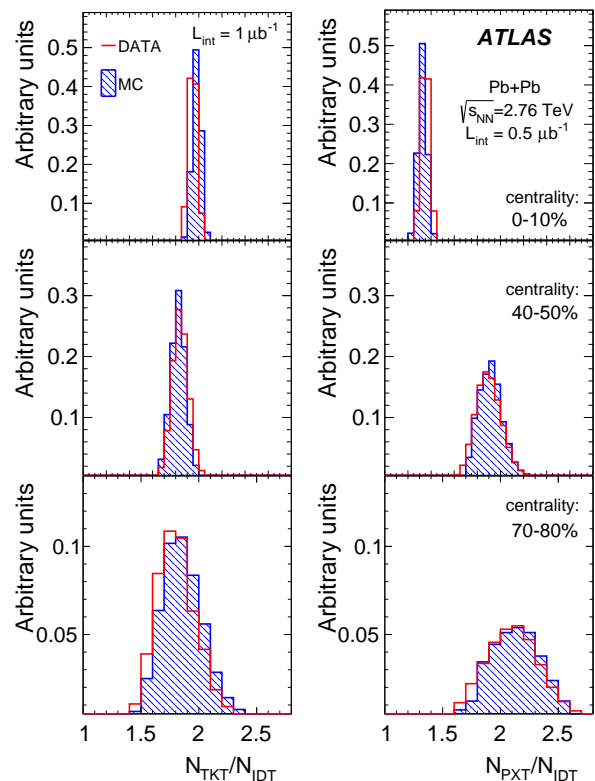


Fig. 6 Comparison of the distribution of multiplicity ratios of number of tracklets, N_{TKT} , (left) and pixel tracks, N_{PXT} , (right) to the number of ID tracks, N_{IDT} , in data (red) and MC simulation (blue) in three centrality bins as indicated on the plots.

6 Corrections to measured v_2

The event-plane method [3] is applied to measure the differential elliptic flow harmonic $v_2(\eta)$ in small η bins with the TKT method, and $v_2(\eta, p_T)$ in small η and p_T bins with the PXT and IDT methods. The differential v_2 measurements are then corrected for detector-related effects.

The first correction is associated with the variation in tracking efficiency induced by the flow itself. It is applied only to the PXT method. The efficiency of the reconstruction was found to depend on detector occupancy, which in turn scales with the particle multiplicity. Since the flow phenomenon is a modulation of the multiplicity, it may induce a variation of the tracking efficiency in an event. Higher occupancy causes lower efficiency, and the number of tracks observed in the event plane is reduced more strongly than the number of tracks observed in other directions. As a consequence, the observed v_2 is smaller. In order to correct for this effect, an appropriate weight was applied to the tracks in the calculation of the numerator of Eq. (2). This weight, the inverted efficiency parameterized as a function of detector occupancy in the vicinity of the track, was derived from MC simulation. In the data, the occupancy was determined for

each track from the number of hits near the track in the first layer of the pixel detector. The corrected $v_2(p_T)$ was compared to the measurement obtained from the IDT method in the same data. In the MC simulation, the comparison was made to $v_2(p_T)$ determined using generated particles. The relative increases in the value of $v_2(p_T)$ in data and in simulation were found to be compatible for $p_T > 0.5$ GeV, the range in which the comparison could be performed.

The occupancy correction results in an increase of about 12% in the integrated v_2 for the 0–20% centrality interval while it amounts to only 1% for the most peripheral collisions, when using a lower p_T integration limit of $p_{T,0} = 0.1$ GeV. For higher values of $p_{T,0}$ the correction gradually becomes smaller. For $p_{T,0} = 0.5$ GeV it decreases to about 7% for the most central collisions.

An additional correction, applied to the differential measurement of v_2 , accounts for the difference between v_2 measured only with fake tracks and v_2 measured with charged-particle tracks from the primary vertex. The corrected v_2 is calculated as

$$v_2 = \frac{v_{2,m} - f v_{2,f}}{1 - f}, \quad (6)$$

where $v_{2,m}$ is the elliptic flow measured with all tracks, $v_{2,f}$ is the flow measured with fake tracks, and f is the fake-track rate. This correction was applied to the differential v_2 measured with the TKT, PXT and IDT methods with the corresponding fake rates and $v_{2,f}$ values. The rate and $v_{2,f}$ of the fake tracks were derived from MC simulation and then cross-checked in the data with a sample, obtained with inverted track selection criteria, in which fake tracks dominate. Differences between the MC simulation and the data of up to 20% were observed and included in the systematic uncertainties.

The fake tracks reduce the values of v_2 integrated over the p_T ranges considered in this analysis. The correction is a function of the fake-track rate and accordingly exhibits a dependence on centrality, p_T and η . For $|\eta| < 1$, the largest correction, about 15%, was obtained for the PXT method with $p_{T,0} = 0.1$ GeV. For peripheral collisions in the same kinematic range, it decreases to about 11%. The correction is smaller for higher values of $p_{T,0}$. It decreases to about 2% for $p_{T,0} = 0.5$ GeV for the 0–10% centrality interval and gradually drops to zero for the most peripheral collisions. The fake-track flow correction for the integrated v_2 obtained with the IDT method ($p_{T,0} = 0.5$ GeV) is less than 2% for the most central collisions and even smaller for the more peripheral ones. For the TKT method, the correction is about 1% for the most central collisions.

The limited p_T resolution for tracks reconstructed in the pixel detector and the rapidly changing dN_{ch}/dp_T distribution lead to a significant bin-to-bin migration in p_T . As a consequence of the variation of v_2 with p_T , v_2 measured in a given p_T bin is contaminated by v_2 values of particles from

the neighbouring bins. In order to compensate for this effect, a correction derived from MC simulation was applied to the $v_2(p_T)$ values. This correction was determined, using pixel tracks matched to generated particles, by comparing the $v_2(p_T)$ distribution as a function of reconstructed p_T to $v_2(p_T)$ as a function of generated p_T . In order to validate the correction derived from the MC simulation, the same procedure was applied in the data and in the simulation in the region of $p_T > 0.5$ GeV, where the ID tracks were used instead of the generated particles. The ID tracks were matched by requiring an angular separation $\sqrt{(\Delta\eta)^2 + (\Delta\phi)^2} < 0.02$. A comparison between the corrections obtained in the data and in the MC simulation, as a function of measured p_T , showed a good agreement.

The correction for p_T -bin migration of the reconstructed tracks was found to be small compared to the occupancy and fake-track flow corrections, and to depend only on the value of $p_{T,0}$. It increases the integrated v_2 value by 1% (1.5%) for $p_{T,0} = 0.1$ GeV ($p_{T,0} = 0.5$ GeV) independently of collision centrality.

7 Uncertainties in the v_2 determination

The systematic uncertainties include those common to different tracking methods, as well as method-specific ones.

The uncertainty which originates from the statistics of the MC samples is treated as a source of systematic uncertainty.

The v_2 values determined for samples enriched in fake tracks in data and MC simulation were compared and differences of up to 20% for both the PXT and IDT methods were observed. For the PXT method, this difference resulted in a change of v_2 , integrated from $p_{T,0} = 0.1$ GeV, for the most central (0–10%) collisions of 3% at mid-rapidity and of 15% at $|\eta| \sim 2$. The impact on the integrated v_2 decreases with increasing centrality. For higher $p_{T,0}$ values, the change was found to be negligible. For the IDT method, the uncertainty on the v_2 value of fake tracks induces a systematic uncertainty in the integrated v_2 for central collisions of less than 4% at mid-rapidity and of 9% at $|\eta| \sim 2$; for peripheral collisions the uncertainty is smaller.

The variation of the fake tracklets' v_2 , at the level of 10%, obtained from the comparison of data and MC simulation, results in an uncertainty at the level of 2% in the integrated v_2 across the centrality range 0–40%.

A comparison of v_2 values obtained with the TKT method for a MC sample with the nominal detector geometry to that with 10% more active material and 15–20% more inactive material shows agreement to better than 2%. Therefore it was assumed that possible inaccuracies in the description of the detector material in the GEANT4 simulation have a negligible effect on the final results. The

same holds for the measurements with the PXT and IDT methods.

An overall scale uncertainty on v_2 originates from the uncertainty on the fraction of the total inelastic cross section accepted by the trigger as well as from the event selection criteria, which affects the population of the centrality bins. It is negligibly small (below 1%) for central collisions and increases to about 6% for the most peripheral collisions for the TKT method and to about 5% for both the PXT and IDT methods.

The influence of the detector nonuniformities on the measured v_2 was checked by comparing the v_2 values obtained for positive and negative η . This led to a typical uncertainty of 1% except for the most peripheral collisions where it increased to about 2%.

Deviations of $\langle \sin 2[\phi - \Psi_2] \rangle$ from zero point to detector non-uniformities and biases in the event-plane determination. The magnitude of the sine term relative to the cosine term is included in the systematic uncertainty of v_2 . For the TKT method, its contribution to the relative systematic uncertainty is negligibly small. For the PXT and IDT methods, it is small for most centrality bins, and increases to 2% only for the most peripheral collisions.

The analysis procedure was checked with MC studies in which the generated elliptic flow signal was compared to the v_2 values obtained with the same analysis chain as used for the data. In this MC closure test, relative differences of up to 2% in central collisions and of up to 5% in peripheral collisions were observed for the TKT method. For the IDT method, the relative difference reaches 2%; for the PXT method, it remains within 2% except for the most peripheral collisions where it increases to 5%. The relative difference between the expected and measured values is included in the total systematic uncertainty.

The ΔR parameter used in the tracklet reconstruction was varied by $\pm 1\sigma$ from the nominal value. The resulting variation in the value of v_2 at the level of 1% is included in the systematic uncertainty. For the PXT and IDT methods, differences between v_2 determined from tracks of negatively and positively charged particles as well as between the baseline v_2 and that obtained with tighter or looser tracking requirements (in which the transverse and longitudinal impact parameter significance criteria are changed by ± 1) also contribute to the systematic uncertainty at the level of a few percent.

For the PXT method, the corrections due to the limited p_T resolution were varied within their statistical uncertainties and the resulting variation was found to be at the level of 0.5%, independently of the centrality.

The p_T spectrum of charged particles in the MC simulation was reweighted so that the expected detector-level distribution agrees with that observed in the data. This changes the effective fake-track rate and therefore the weights used

Source	Centrality bin				
	0–10%	10–20%	20–60%	60–70%	70–80%
	TKT $p_T > 0.07$ GeV				
MC Statistics	0.1	0.1	<0.2	0.3	1
Fake tracks	2	2	1–2	1	1
Centrality bins	1	1.5	<1	2	6
N-P η regions	2	1	<1.5	1	2.5
Sine term	1.5	1	1	1	1
Closure	1.5	1	<2	3.5	5
ΔR	1	0.5	<1	0.5	1
Total	3.5	3.2	<3.2	4	8
	PXT $p_T > 0.1$ GeV				
MC Statistics	0.1	0.1	<0.2	0.3	1
Fake tracks	3	2	<1.5	0.5	0.5
Centrality bins	1	1.5	<1	1.5	5
N-P η regions	0.5	0.5	<0.5	1	3
Sine term	0.5	0	<0.5	1	4
Closure	1	1	<2	0	5
Charge \pm	0.5	0.5	<1	1	1.5
Track selection	0.5	0.5	<0.5	1	1
p_T resolution	0.5	0.5	0.5	0.5	0.5
Total	3	2	<2	2	8
	IDT $p_T > 0.5$ GeV				
MC Statistics	0.1	0.1	<0.2	0.3	1
Fake tracks	3.5	1.5	<1	0.2	0.2
Centrality bins	1	1.5	<1	1	5
N-P η regions	1.2	1	<1.5	0.5	0.5
Sine term	0.5	0.5	0.5	0.5	1.5
Closure	1.5	0.5	<1	0.5	0.5
Charge \pm	0.2	0.2	0.2	0.2	2.2
Track selection	0.5	0	<0.5	0.2	1
Total	3.5	2	<1.5	1	5.5

Table 1 Summary of the systematic uncertainties as percentages of the integrated v_2 value for charged particles with $|\eta| < 1$ and different collision centrality bins.

in the calculation of v_2 . A variation of these weights by up to 10% has a negligible effect on the determination of v_2 .

The different contributions to the total systematic uncertainty on the integrated v_2 for $|\eta| < 1$ are shown in Fig. 7 and summarized in Table 1 for the three tracking methods. The total systematic uncertainties are determined by adding in quadrature all the individual contributions and are treated as $\pm 1\sigma$ uncertainties.

8 Results

Figure 8 shows the centrality dependence of v_2 integrated over $|\eta| < 1$. For the TKT method, v_2 is integrated over $p_T > 0.07$ GeV. For the PXT method, v_2 is integrated over $p_{T,0} < p_T < 5$ GeV and $p_{T,0}$ is varied from 0.1 GeV to 0.5 GeV in steps of 0.1 GeV. Also shown is the v_2 value obtained from the IDT method integrated over $0.5 < p_T < 5$ GeV. The TKT method with $p_{T,0} = 0.07$ GeV gives results consistent with the v_2 values obtained with the PXT method with $p_{T,0} = 0.1$ GeV, as could be expected due to the very low charged-particle density and small v_2 signal in the momentum range

below 0.1 GeV. This indicates that there is no need to extrapolate the measurements obtained with tracklets down to $p_T = 0$ in order to obtain a reliable estimate of v_2 integrated over the whole kinematic range in p_T . Furthermore, for the PXT method such an extrapolation would result in a very small correction to the measured integrated flow, well within the uncertainties of the measurement. This is in contrast to the integrated v_2 with $p_{T,0}$ chosen at higher values, as also shown in Fig. 8. It can be seen that the integrated v_2 in-

creases almost linearly with $p_{T,0}$ for $p_{T,0} > 0.1$ GeV. Good agreement between the PXT and IDT methods is observed at $p_{T,0} = 0.5$ GeV.

In Fig. 9, the results of this analysis are compared to the integrated v_2 measured by CMS [20] with $p_{T,0} = 0.3$ GeV. In this comparison, the sensitivity to $p_{T,0}$ is clearly visible. A systematically larger v_2 is observed for the higher value of $p_{T,0}$ as a consequence of the strong increase of v_2 with increasing p_T .

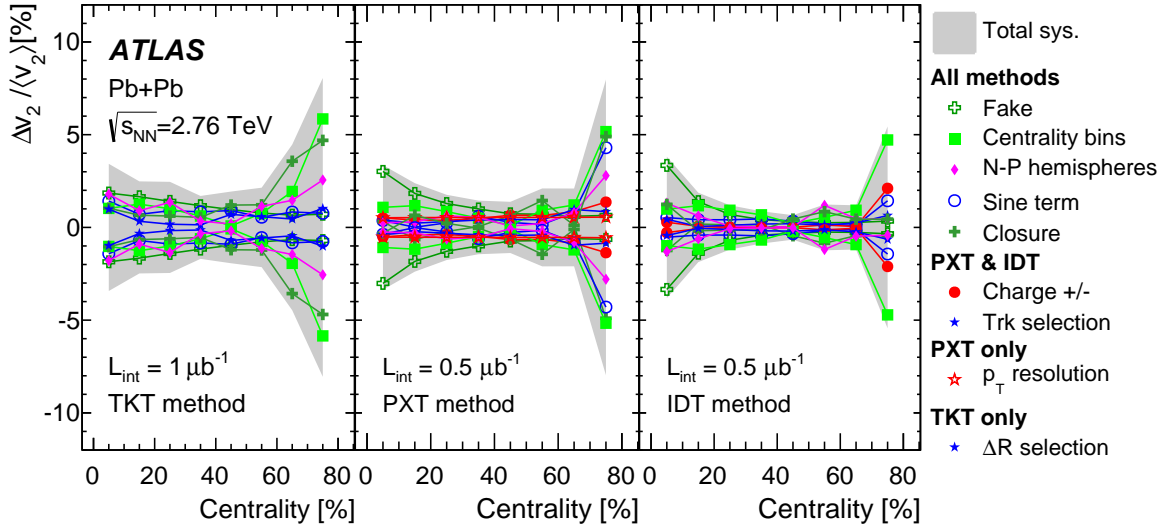


Fig. 7 Contributions to the relative systematic uncertainty on the elliptic flow, $\Delta v_2 / \langle v_2 \rangle$, as a function of centrality for $|\eta| < 1$ with the TKT (left), PXT (centre) and IDT (right) methods. The integration limits for the three methods are 0.07, 0.1, 0.5 GeV, respectively. The total uncertainty is indicated by the shaded area. The individual contributions, are described in the legend and explained in the text.

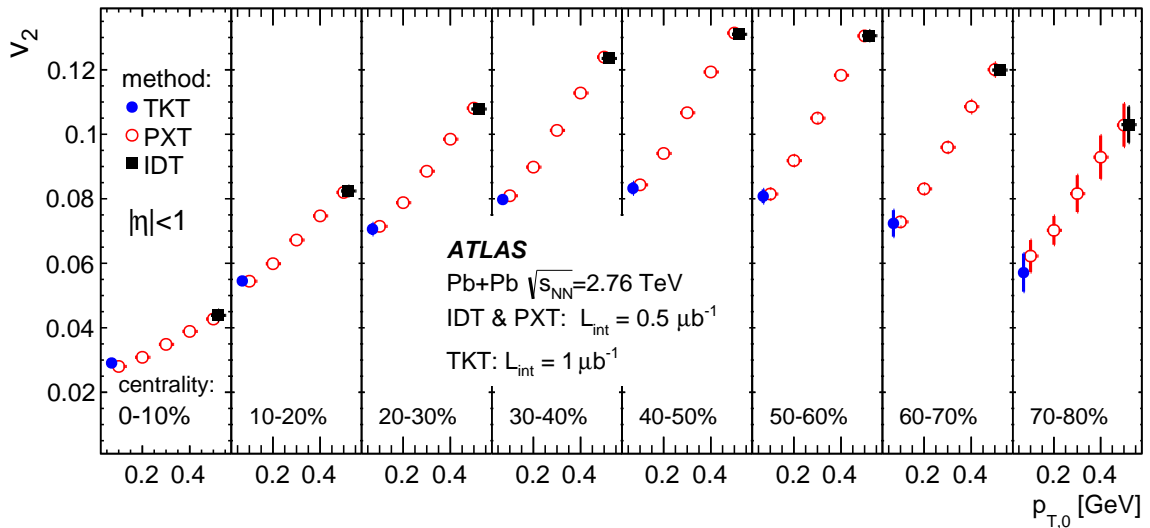


Fig. 8 Elliptic flow v_2 integrated over transverse momentum $p_T > p_{T,0}$ as a function of $p_{T,0}$ for different centrality intervals, obtained with different charged-particle reconstruction methods: the tracklet (TKT) method with $p_{T,0} = 0.07$ GeV, the pixel track (PXT) method with $p_{T,0} \geq 0.1$ GeV and the ID track (IDT) method with $p_{T,0} = 0.5$ GeV as described in the legend. Error bars show statistical and systematic uncertainties added in quadrature.

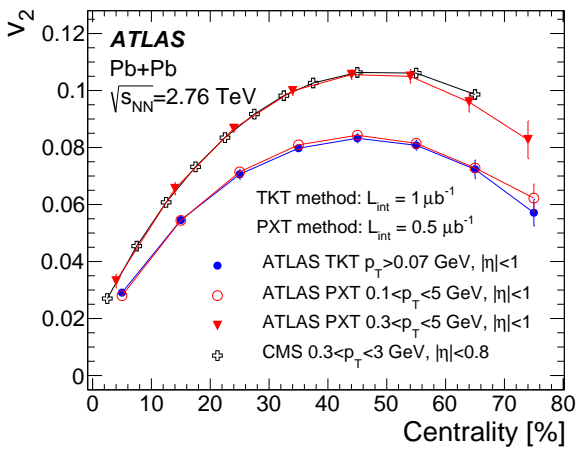


Fig. 9 Centrality dependence of elliptic flow, v_2 , measured for $|\eta| < 1$ and integrated over transverse momenta, p_T , for different charged-particle reconstruction methods as described in the legend. Also shown are v_2 measurements by CMS integrated over $0.3 < p_T < 5$ GeV and $|\eta| < 0.8$ [20] (open crosses). Error bars show statistical and systematic uncertainties added in quadrature.

The η dependence of the p_T -integrated v_2 provides useful constraints on the initial conditions of heavy-ion collisions used in model descriptions of the system's evolution (see, e.g., Refs [1, 2]). Figure 10 shows the η dependence of the p_T -integrated v_2 . As already shown in Fig. 9, the difference between the results obtained with $p_{T,0}$ values of 0.07 GeV and 0.1 GeV is very small and the two measurements agree within uncertainties. The results obtained using the PXT and IDT methods for the same $p_{T,0}$ are also consistent. The η dependence of the integrated v_2 is very weak. A decrease with increasing $|\eta|$ of about 5–10% is seen. A comparison with the results from the CMS experiment [20] is shown in Fig. 11 for the 40–50% centrality interval. The ATLAS measurements performed with the PXT method were integrated over p_T for different $p_{T,0}$ values, including one adjusted to match that used by CMS. The results agree, within uncertainties, provided the same $p_{T,0}$ is used.

The different upper limits in the p_T integration, 3 GeV for CMS and 5 GeV for ATLAS, have negligible effect on the integrated v_2 value. A systematic decrease in v_2 with decreasing $p_{T,0}$ is observed as expected from the linear dependence of v_2 on p_T for $p_T \approx 0$. The decreasing value of $p_{T,0}$ together with that of v_2 makes the integration over the full p_T range less sensitive to the uncertainties in the extrapolation down to $p_T = 0$.

The large acceptance in η of the ATLAS and CMS experiments makes it possible to study whether the observation of the extended longitudinal scaling of v_2 , when viewed in the rest frame of one of the colliding nuclei, reported by the PHOBOS experiment at RHIC [6, 32], holds at the much higher LHC energy. The PHOBOS mea-

surements of elliptic flow over a range of Au+Au collision energies, $\sqrt{s_{NN}} = 19.6, 62.4, 130$ and 200 GeV, showed energy independence of the integrated v_2 as a function of $|\eta| - y_{\text{beam}}$, where $y_{\text{beam}} = \ln(\sqrt{s_{NN}}/m)$ is the beam rapidity and m is the proton mass. A similar effect was also observed in charged-particle densities [6] and is known as limiting fragmentation [33]. In Fig. 12, the integrated v_2 is plotted as a function of $|\eta| - y_{\text{beam}}$ and compared to the PHOBOS results for three centrality bins matching those used by PHOBOS. The PHOBOS results are obtained with the event-plane method for charged particles with a low- p_T limit of 0.035 GeV at mid-rapidity and of 0.004 GeV around the beam rapidity [34]. The CMS data [20] obtained with the event-plane method are also shown. The CMS measurement represents v_2 integrated over p_T from 0 to 3 GeV. This measurement was obtained by extrapolating $v_2(p_T)$ measured for $p_T > 0.3$ GeV and the charged-particle spectra down to $p_T = 0$ under the assumption that $v_2(p_T = 0) = 0$ and with the charged-particle yield constrained by the measured $dN_{\text{ch}}/d\eta$ distribution [35].

The ATLAS and CMS results are shifted systematically by up to 5% while the uncertainties of ATLAS measurement are of the order of 3–5% and CMS are of the order of 5–6%. However, as can be seen from the figure, there is no overlap in $|\eta| - y_{\text{beam}}$ between the PHOBOS and LHC data, so a direct comparison with the low-energy data is not possible. Nevertheless, it can be concluded, keeping in mind the relatively large uncertainties in the low-energy results, that the extrapolation of the trend observed at RHIC to the LHC energy appears to be consistent with the LHC measurements, although the dependence on $|\eta| - y_{\text{beam}}$ may be weaker at the LHC energy.

9 Summary and conclusions

Measurements of the integrated elliptic flow of charged particles in Pb+Pb collisions at $\sqrt{s_{NN}} = 2.76$ TeV are presented by the ATLAS experiment at the LHC. The elliptic anisotropy parameter v_2 is measured with the event-plane method over a broad range of collision centralities (0–80%). The kinematic range in pseudorapidity extends out to $|\eta| = 2.5$, and in p_T down to 0.07 GeV. This low- p_T region is reached by using a tracklet reconstruction algorithm to analyze about $1 \mu\text{b}^{-1}$ of data taken with the solenoid field turned off. Other track reconstruction methods with low- p_T thresholds of 0.1 GeV and 0.5 GeV respectively, are exploited in order to verify the tracklet measurement and provide results that can be directly compared to other LHC measurements. The values of v_2 integrated from $p_T = 0.07$ GeV and from $p_T = 0.1$ GeV agree with each other to better than 4%, which proves that the contribution from tracks with p_T below 0.1 GeV is negligible and

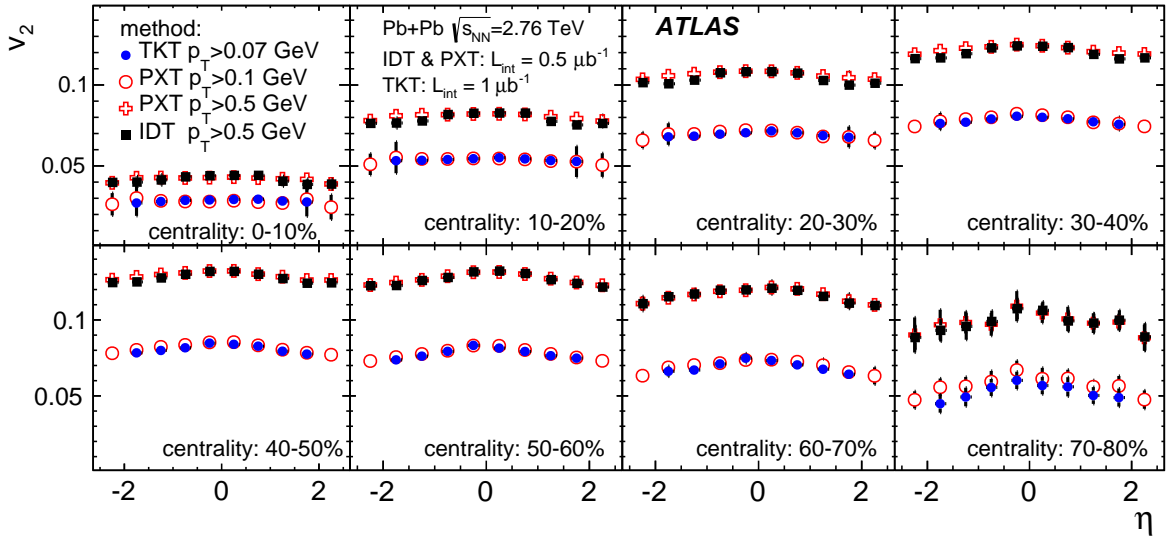


Fig. 10 Pseudorapidity, η , dependence of elliptic flow, v_2 , integrated over transverse momentum, p_T , for different charged particle reconstruction methods and different low- p_T thresholds in different centrality intervals as indicated in the legend. Error bars show statistical and systematic uncertainties added in quadrature.

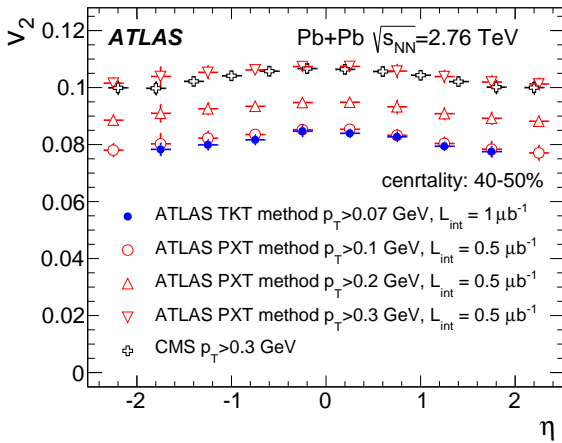


Fig. 11 Comparison of the pseudorapidity, η , dependence of elliptic flow, v_2 , integrated over transverse momentum, p_T , for different low- p_T thresholds, as indicated in the legend, in the 40–50% centrality interval from the ATLAS and CMS experiments. Error bars show statistical and systematic uncertainties added in quadrature.

therefore no model-dependent extrapolation to $p_T=0$ is necessary.

The p_T -integrated elliptic flow as a function of collision centrality shows a clear dependence on $p_{T,0}$, both within the present measurements and in comparison to the CMS results obtained with higher low- p_T limits. The integrated elliptic flow increases with centrality, reaching a maximum of 0.08 for mid-central collisions (40–50%) and then decreases to about 0.02 for the most central collisions.

The pseudorapidity dependence of the p_T -integrated v_2 is very weak, with a slight decrease in v_2 as $|\eta|$ increases. The results are in agreement with the CMS measurements covering the same η range, provided the same low- p_T cutoff is used. The integrated v_2 transformed to the rest frame of one of the colliding nuclei is compared to the lower-energy RHIC data. Although a direct comparison is not possible due to the non-overlapping kinematic regions, the general trend observed in the RHIC energy regime seems consistent with the LHC measurements, while the latter may have a weaker dependence on pseudorapidity.

10 Acknowledgements

We thank CERN for the very successful operation of the LHC, as well as the support staff from our institutions without whom ATLAS could not be operated efficiently.

We acknowledge the support of ANPCyT, Argentina; YerPhI, Armenia; ARC, Australia; BMWF and FWF, Austria; ANAS, Azerbaijan; SSTC, Belarus; CNPq and FAPESP, Brazil; NSERC, NRC and CFI, Canada; CERN; CONICYT, Chile; CAS, MOST and NSFC, China; COLCIENCIAS, Colombia; MSMT CR, MPO CR and VSC CR, Czech Republic; DNRF, DNSRC and Lundbeck Foundation, Denmark; EPLANET, ERC and NSRF, European Union; IN2P3-CNRS, CEA-DSM/IRFU, France; GNSF, Georgia; BMBF, DFG, HGF, MPG and AvH Foundation, Germany; GSRT and NSRF, Greece; ISF, MINERVA, GIF, I-CORE and Benozziyo Center, Israel; INFN, Italy; MEXT and JSPS, Japan; CNRST, Morocco; FOM and NWO,

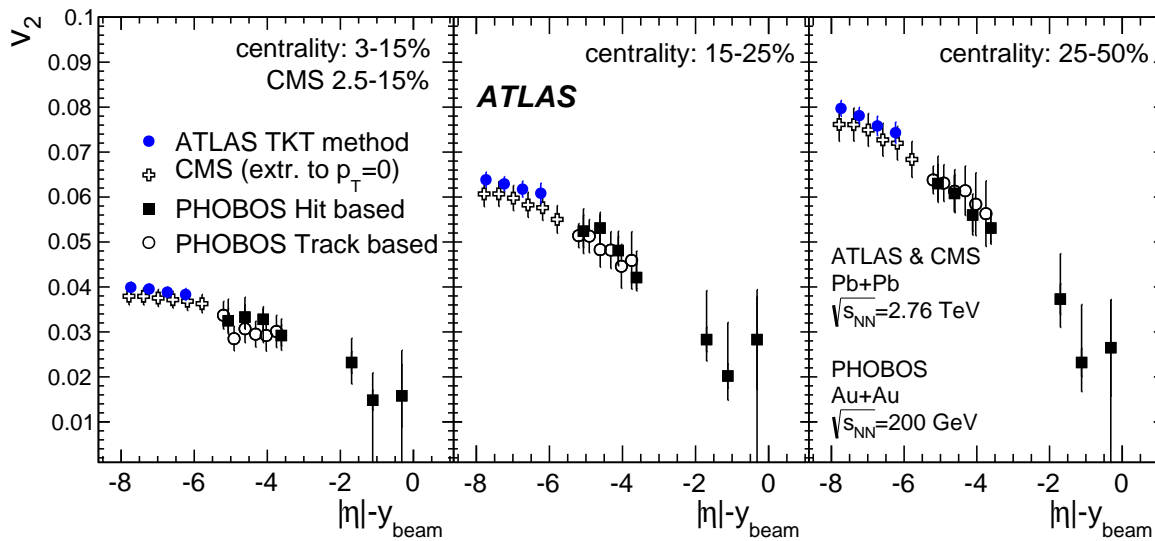


Fig. 12 Integrated elliptic flow, v_2 , as a function of $|\eta| - y_{\text{beam}}$ for three centrality intervals indicated in the legend, measured by the ATLAS and CMS experiments for Pb+Pb collisions at 2.76 TeV and by the PHOBOS experiment for Au+Au collisions at 200 GeV. The CMS result is obtained by averaging the $v_2(p_T)$ with the charged particle spectra over the range $0 < p_T < 3$ GeV. Error bars show statistical and systematic uncertainties added in quadrature.

Netherlands; BRF and RCN, Norway; MNI SW and NCN, Poland; GRICES and FCT, Portugal; MNE/IFA, Romania; MES of Russia and ROSATOM, Russian Federation; JINR; MSTD, Serbia; MSSR, Slovakia; ARRS and MIZŠ, Slovenia; DST/NRF, South Africa; MINECO, Spain; SRC and Wallenberg Foundation, Sweden; SER, SNSF and Cantons of Bern and Geneva, Switzerland; NSC, Taiwan; TAEK, Turkey; STFC, the Royal Society and Leverhulme Trust, United Kingdom; DOE and NSF, United States of America.

The crucial computing support from all WLCG partners is acknowledged gratefully, in particular from CERN and the ATLAS Tier-1 facilities at TRIUMF (Canada), NDGF (Denmark, Norway, Sweden), CC-IN2P3 (France), KIT/GridKA (Germany), INFN-CNAF (Italy), NL-T1 (Netherlands), PIC (Spain), ASGC (Taiwan), RAL (UK) and BNL (USA) and in the Tier-2 facilities worldwide.

References

1. P. Romatschke, *Int. J. Mod. Phys. E* **19**, 1 (2010). [arXiv:0902.3663]
2. T. Hirano, U.W. Heinz, D. Kharzeev, R. Lacey, Y. Nara, *Phys. Lett. B* **636**, 299 (2006). [arXiv:nucl-th/0511046]
3. A.M. Poskanzer, S. Voloshin, *Phys. Rev. C* **58**, 1671 (1998). [arXiv:nucl-ex/9805001]
4. ATLAS Collaboration, *JHEP* **1311**, 183 (2013). [arXiv:1305.2942]
5. BRAHMS Collaboration, I. Arsene, et al., *Nucl. Phys. A* **757**, 1 (2005). [arXiv:nucl-ex/0410020]
6. PHOBOS Collaboration, B.B. Back et al., *Nucl. Phys. A* **757**, 28 (2005). [arXiv:nucl-ex/0410022]
7. STAR Collaboration, J. Adams et al., *Nucl. Phys. A* **757**, 102 (2005). [arXiv:nucl-ex/0501009]
8. PHENIX Collaboration, K. Adcox et al., *Nucl. Phys. A* **757**, 184 (2005). [arXiv:nucl-ex/0410003]
9. G. Kestin, U.W. Heinz, *Eur. Phys. J. C* **61**, 545 (2009). [arXiv:0806.4539]
10. M. Chojnacki, W. Florkowski, W. Broniowski, A. Kisiel, *Phys. Rev. C* **78**, 014905 (2008). [arXiv:0712.0947]
11. P. Romatschke, U. Romatschke, *Phys. Rev. Lett.* **99**, 172301 (2007). [arXiv:0706.1522]
12. B.H. Alver, C. Gombeaud, M. Luzum, J.Y. Ollitrault, *Phys. Rev. C* **82**, 034913 (2010). [arXiv:1007.5469]
13. U.W. Heinz, J.S. Moreland, H. Song, *Phys. Rev. C* **80**, 061901 (2009). [arXiv:0908.2617]
14. H. Song, U.W. Heinz, *Phys. Rev. C* **81**, 024905 (2010). [arXiv:0909.1549]
15. Z. Qiu, C. Shen, U.W. Heinz, *Phys. Lett. B* **707**, 151 (2012). [arXiv:1110.3033]
16. ALICE Collaboration, K. Aamodt et al., *Phys. Rev. Lett.* **105**, 252302 (2010). [arXiv:1011.3914]
17. ALICE Collaboration, K. Aamodt et al., *Phys. Rev. Lett.* **107**, 032301 (2011). [arXiv:1105.3865]
18. ATLAS Collaboration, *Phys. Lett. B* **707**, 330 (2012). [arXiv:1108.6018]
19. ATLAS Collaboration, *Phys. Rev. C* **86**, 014907 (2012). [arXiv:1203.3087]

20. CMS Collaboration, Phys. Rev. C **87**, 014902 (2013). [arXiv:1204.1409]
21. CMS Collaboration, Phys. Rev. Lett. **109**, 022301 (2012). [arXiv:1204.1850]
22. B. Schenke, S. Jeon, C. Gale, Phys. Rev. Lett. **106**, 042301 (2011). [arXiv:1009.3244]
23. P. Bozek, Phys. Rev. C **85**, 034901 (2012). [arXiv:1110.6742]
24. ATLAS Collaboration, JINST **3**, S08003 (2008)
25. M. Gyulassy, X.N. Wang, Comput. Phys. Commun. **83**, 307 (1994). [arXiv:nucl-th/9502021]
26. ATLAS Collaboration, Eur. Phys. J. C **70**, 823 (2010). [arXiv:1005.4568]
27. S. Agostinelli, et al., Nucl. Instr. Meth. A **506**, 250 (2003)
28. ATLAS Collaboration, Phys. Lett. B **710**, 363 (2012). [arXiv:1108.6027]
29. ATLAS Collaboration, Phys. Lett. B **688**, 21 (2010). [arXiv:1003.3124]
30. ATLAS Collaboration, New J. Phys. **13**, 053033 (2011). [arXiv:1012.5104]
31. ALICE Collaboration, B. Abelev et al., Phys. Rev. C **88**, 044910 (2013). [arXiv:1303.0737]
32. PHOBOS Collaboration, B.B. Back et al., Phys. Rev. C **72**, 051901 (2005). [arXiv:nucl-ex/0407012]
33. J. Benecke, T.T. Chou, C.N. Yang, E. Yen, Phys. Rev. **188**, 2159 (1969)
34. PHOBOS Collaboration, B.B. Back et al., Phys. Rev. C **74**, 021901 (2006). [arXiv:nucl-ex/0509034]
35. CMS Collaboration, JHEP **1108**, 141 (2011). [arXiv:1107.4800]

Appendix

In the low- p_T region, the track reconstruction efficiency depends strongly on the particle type. This information is important for comparison of measurements with theory predictions in which the elliptic flow depends on the particle type.

The efficiency of the PXT and TKT methods in reconstructing tracks with $|\eta| < 1$ generated as π^\pm , K^\pm , p , and \bar{p} in MC simulation is shown in Fig. 13 as a function of p_T . Large differences in efficiency are observed for the PXT method at p_T below about 1 GeV and for the TKT method at p_T below about 0.4 GeV. Above these values, the reconstruction efficiency is independent of particle type. The efficiency is lowest for p and \bar{p} . For the TKT method, which is most relevant at low p_T , the efficiency for reconstructing protons drops to zero below 0.2 GeV.

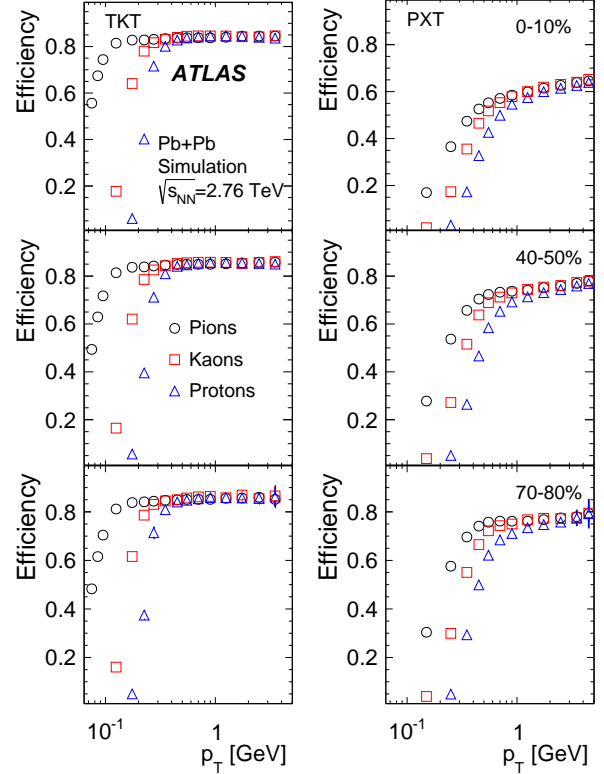


Fig. 13 The transverse momentum, p_T , dependence of the TKT (left) and PXT (right) track reconstruction efficiency for π^\pm , K^\pm and p^\pm in the pseudorapidity range $|\eta| < 1$ for three centrality intervals, as indicated in the legend.

The ATLAS Collaboration

G. Aad⁸⁴, B. Abbott¹¹², J. Abdallah¹⁵²,
 S. Abdel Khalek¹¹⁶, O. Abdinov¹¹, R. Aben¹⁰⁶, B. Abi¹¹³,
 M. Abolins⁸⁹, O.S. AbouZeid¹⁵⁹, H. Abramowicz¹⁵⁴,
 H. Abreu¹³⁷, R. Abreu³⁰, Y. Abulaiti^{147a,147b},
 B.S. Acharya^{165a,165b,a}, L. Adamczyk^{38a}, D.L. Adams²⁵,
 J. Adelman¹⁷⁷, S. Adomeit⁹⁹, T. Adye¹³⁰,
 T. Agatonovic-Jovin^{13b}, J.A. Aguilar-Saavedra^{125f,125a},
 M. Agustoni¹⁷, S.P. Ahlen²², F. Ahmadov^{64,b},
 G. Aielli^{134a,134b}, T.P.A. Åkesson⁸⁰, G. Akimoto¹⁵⁶,
 A.V. Akimov⁹⁵, G.L. Alberghi^{20a,20b}, J. Albert¹⁷⁰,
 S. Albrand⁵⁵, M.J. Alconada Verzini⁷⁰, M. Aleksa³⁰,
 I.N. Aleksandrov⁶⁴, C. Alexa^{26a}, G. Alexander¹⁵⁴,
 G. Alexandre⁴⁹, T. Alexopoulos¹⁰, M. Alhroob^{165a,165c},
 G. Alimonti^{90a}, L. Alio⁸⁴, J. Alison³¹, B.M.M. Allbrooke¹⁸,
 L.J. Allison⁷¹, P.P. Allport⁷³, S.E. Allwood-Spiers⁵³,
 J. Almond⁸³, A. Aloisio^{103a,103b}, A. Alonso³⁶, F. Alonso⁷⁰,
 C. Alpigiani⁷⁵, A. Altheimer³⁵, B. Alvarez Gonzalez⁸⁹,
 M.G. Alviggi^{103a,103b}, K. Amako⁶⁵, Y. Amaral Coutinho^{24a},
 C. Amelung²³, D. Amidei⁸⁸, S.P. Amor Dos Santos^{125a,125c},
 A. Amorim^{125a,125b}, S. Amoroso⁴⁸, N. Amram¹⁵⁴,
 G. Amundsen²³, C. Anastopoulos¹⁴⁰, L.S. Ancu⁴⁹,
 N. Andari³⁰, T. Andeen³⁵, C.F. Anders^{58b}, G. Anders³⁰,
 K.J. Anderson³¹, A. Andreazza^{90a,90b}, V. Andrei^{58a},
 X.S. Anduaga⁷⁰, S. Angelidakis⁹, I. Angelozzi¹⁰⁶,
 P. Anger⁴⁴, A. Angerami³⁵, F. Anghinolfi³⁰,
 A.V. Anisenkov¹⁰⁸, N. Anjos^{125a}, A. Annovi⁴⁷,
 A. Antonaki⁹, M. Antonelli⁴⁷, A. Antonov⁹⁷, J. Antos^{145b},
 F. Anulli^{133a}, M. Aoki⁶⁵, L. Aperio Bella¹⁸, R. Apolle^{119,c},
 G. Arabidze⁸⁹, I. Aracena¹⁴⁴, Y. Arai⁶⁵, J.P. Araque^{125a},
 A.T.H. Arce⁴⁵, J-F. Arguin⁹⁴, S. Argyropoulos⁴²,
 M. Arik^{19a}, A.J. Armbruster³⁰, O. Arnaez⁸², V. Arnal⁸¹,
 H. Arnold⁴⁸, O. Arslan²¹, A. Artamonov⁹⁶, G. Artoni²³,
 S. Asai¹⁵⁶, N. Asbah⁹⁴, A. Ashkenazi¹⁵⁴, S. Ask²⁸,
 B. Åsman^{147a,147b}, L. Asquith⁶, K. Assamagan²⁵,
 R. Astalos^{145a}, M. Atkinson¹⁶⁶, N.B. Atlay¹⁴²,
 B. Auerbach⁶, K. Augsten¹²⁷, M. Aourousseau^{146b},
 G. Avolio³⁰, G. Azuelos^{94,d}, Y. Azuma¹⁵⁶, M.A. Baak³⁰,
 C. Bacci^{135a,135b}, H. Bachacou¹³⁷, K. Bachas¹⁵⁵,
 M. Backes³⁰, M. Backhaus³⁰, J. Backus Mayes¹⁴⁴,
 E. Badescu^{26a}, P. Bagiacchi^{133a,133b}, P. Bagnaia^{133a,133b},
 Y. Bai^{33a}, T. Bain³⁵, J.T. Baines¹³⁰, O.K. Baker¹⁷⁷,
 S. Baker⁷⁷, P. Balek¹²⁸, F. Balli¹³⁷, E. Banas³⁹,
 Sw. Banerjee¹⁷⁴, A. Bangert¹⁵¹, A.A.E. Bannoura¹⁷⁶,
 V. Bansal¹⁷⁰, H.S. Bansil¹⁸, L. Barak¹⁷³, S.P. Baranov⁹⁵,
 E.L. Barberio⁸⁷, D. Barberis^{50a,50b}, M. Barbero⁸⁴,
 T. Barillari¹⁰⁰, M. Barisonzi¹⁷⁶, T. Barklow¹⁴⁴,
 N. Barlow²⁸, B.M. Barnett¹³⁰, R.M. Barnett¹⁵,
 Z. Barnovska⁵, A. Baroncelli^{135a}, G. Barone⁴⁹,
 A.J. Barr¹¹⁹, F. Barreiro⁸¹,
 J. Barreiro Guimarães da Costa⁵⁷, R. Bartoldus¹⁴⁴,
 A.E. Barton⁷¹, P. Bartos^{145a}, V. Bartsch¹⁵⁰, A. Bassalat¹¹⁶,
 A. Basye¹⁶⁶, R.L. Bates⁵³, L. Batkova^{145a}, J.R. Batley²⁸,
 M. Battistin³⁰, F. Bauer¹³⁷, H.S. Bawa^{144,e}, T. Beau⁷⁹,
 P.H. Beauchemin¹⁶², R. Beccherle^{123a,123b}, P. Bechtel²¹,
 H.P. Beck¹⁷, K. Becker¹⁷⁶, S. Becker⁹⁹,
 M. Beckingham¹³⁹, C. Becot¹¹⁶, A.J. Beddall^{19c},
 A. Beddall^{19c}, S. Bedikian¹⁷⁷, V.A. Bednyakov⁶⁴,
 C.P. Bee¹⁴⁹, L.J. Beamster¹⁰⁶, T.A. Beermann¹⁷⁶,
 M. Begel²⁵, K. Behr¹¹⁹, C. Belanger-Champagne⁸⁶,
 P.J. Bell⁴⁹, W.H. Bell⁴⁹, G. Bella¹⁵⁴, L. Bellagamba^{20a},
 A. Bellerive²⁹, M. Bellomo⁸⁵, A. Belloni⁵⁷, K. Belotskiy⁹⁷,
 O. Beltramello³⁰, O. Benary¹⁵⁴, D. Bencheikroun^{136a},
 K. Bendtz^{147a,147b}, N. Benekos¹⁶⁶, Y. Benhammou¹⁵⁴,
 E. Benhar Noccioli⁴⁹, J.A. Benitez Garcia^{160b},
 D.P. Benjamin⁴⁵, J.R. Bensinger²³, K. Benslama¹³¹,
 S. Bentvelsen¹⁰⁶, D. Berge¹⁰⁶, E. Bergeas Kuutmann¹⁶,
 N. Berger⁵, F. Berghaus¹⁷⁰, E. Berglund¹⁰⁶, J. Beringer¹⁵,
 C. Bernard²², P. Bernal⁷⁷, C. Bernius⁷⁸,
 F.U. Bernlochner¹⁷⁰, T. Berry⁷⁶, P. Berta¹²⁸, C. Bertella⁸⁴,
 F. Bertolucci^{123a,123b}, M.I. Besana^{90a}, G.J. Besjes¹⁰⁵,
 O. Bessidskaia^{147a,147b}, N. Besson¹³⁷, C. Betancourt⁴⁸,
 S. Bethke¹⁰⁰, W. Bhimji⁴⁶, R.M. Bianchi¹²⁴,
 L. Bianchini²³, M. Bianco³⁰, O. Biebel⁹⁹, S.P. Bieniek⁷⁷,
 K. Bierwagen⁵⁴, J. Biesiada¹⁵, M. Biglietti^{135a},
 J. Bilbao De Mendizabal⁴⁹, H. Bilokon⁴⁷, M. Bindi⁵⁴,
 S. Binet¹¹⁶, A. Bingul^{19c}, C. Bini^{133a,133b}, C.W. Black¹⁵¹,
 J.E. Black¹⁴⁴, K.M. Black²², D. Blackburn¹³⁹, R.E. Blair⁶,
 J.-B. Blanchard¹³⁷, T. Blazek^{145a}, I. Bloch⁴², C. Blocker²³,
 W. Blum^{82,*}, U. Blumenschein⁵⁴, G.J. Bobbink¹⁰⁶,
 V.S. Bobrovnikov¹⁰⁸, S.S. Bocchetta⁸⁰, A. Bocci⁴⁵,
 C.R. Boddy¹¹⁹, M. Boehler⁴⁸, J. Boek¹⁷⁶, T.T. Boek¹⁷⁶,
 J.A. Bogaerts³⁰, A.G. Bogdanichikov¹⁰⁸, A. Bogouch^{91,*},
 C. Bohm^{147a}, J. Bohm¹²⁶, V. Boisvert⁷⁶, T. Bold^{38a},
 V. Boldea^{26a}, A.S. Boldyrev⁹⁸, M. Bomben⁷⁹, M. Bona⁷⁵,
 M. Boonekamp¹³⁷, A. Borisov¹²⁹, G. Borissov⁷¹,
 M. Borri⁸³, S. Borroni⁴², J. Bortfeldt⁹⁹,
 V. Bortolotto^{135a,135b}, K. Bos¹⁰⁶, D. Boscherini^{20a},
 M. Bosman¹², H. Boterenbrood¹⁰⁶, J. Boudreau¹²⁴,
 J. Bouffard², E.V. Bouhova-Thacker⁷¹, D. Boumediene³⁴,
 C. Bourdarios¹¹⁶, N. Bousson¹¹³, S. Boutouil^{136d},
 A. Boveia³¹, J. Boyd³⁰, I.R. Boyko⁶⁴,
 I. Bozovic-Jelisavcic^{13b}, J. Bracinik¹⁸, P. Branchini^{135a},
 A. Brandt⁸, G. Brandt¹⁵, O. Brandt^{58a}, U. Bratzler¹⁵⁷,
 B. Brau⁸⁵, J.E. Brau¹¹⁵, H.M. Braun^{176,*},
 S.F. Brazzale^{165a,165c}, B. Brelier¹⁵⁹, K. Brendlinger¹²¹,
 A.J. Brennan⁸⁷, R. Brenner¹⁶⁷, S. Bressler¹⁷³,
 K. Bristow^{146c}, T.M. Bristow⁴⁶, D. Britton⁵³,
 F.M. Brochu²⁸, I. Brock²¹, R. Brock⁸⁹, C. Bromberg⁸⁹,
 J. Bronner¹⁰⁰, G. Brooijmans³⁵, T. Brooks⁷⁶,
 W.K. Brooks^{32b}, J. Brosamer¹⁵, E. Brost¹¹⁵, G. Brown⁸³,
 J. Brown⁵⁵, P.A. Bruckman de Renstrom³⁹,
 D. Bruncko^{145b}, R. Bruneliere⁴⁸, S. Brunet⁶⁰, A. Bruni^{20a},
 G. Bruni^{20a}, M. Bruschi^{20a}, L. Bryngemark⁸⁰, T. Buanes¹⁴,
 Q. Buat¹⁴³, F. Bucci⁴⁹, P. Buchholz¹⁴²,

- R.M. Buckingham¹¹⁹, A.G. Buckley⁵³, S.I. Buda^{26a},
I.A. Budagov⁶⁴, F. Buehrer⁴⁸, L. Bugge¹¹⁸, M.K. Bugge¹¹⁸,
O. Bulekov⁹⁷, A.C. Bundock⁷³, H. Burckhart³⁰,
S. Burdin⁷³, B. Burghgrave¹⁰⁷, S. Burke¹³⁰,
I. Burmeister⁴³, E. Busato³⁴, D. Büscher⁴⁸, V. Büscher⁸²,
P. Bussey⁵³, C.P. Buszello¹⁶⁷, B. Butler⁵⁷, J.M. Butler²²,
A.I. Butt³, C.M. Buttar⁵³, J.M. Butterworth⁷⁷, P. Butti¹⁰⁶,
W. Buttinger²⁸, A. Buzatu⁵³, M. Byszewski¹⁰,
S. Cabrera Urbán¹⁶⁸, D. Caforio^{20a,20b}, O. Cakir^{4a},
P. Calafiura¹⁵, A. Calandri¹³⁷, G. Calderini⁷⁹, P. Calfayan⁹⁹,
R. Calkins¹⁰⁷, L.P. Caloba^{24a}, D. Calvet³⁴, S. Calvet³⁴,
R. Camacho Toro⁴⁹, S. Camarda⁴², D. Cameron¹¹⁸,
L.M. Caminada¹⁵, R. Caminal Armadans¹², S. Campana³⁰,
M. Campanelli⁷⁷, A. Campoverde¹⁴⁹, V. Canale^{103a,103b},
A. Canepa^{160a}, J. Cantero⁸¹, R. Cantrill⁷⁶, T. Cao⁴⁰,
M.D.M. Capeans Garrido³⁰, I. Caprini^{26a}, M. Caprini^{26a},
M. Capua^{37a,37b}, R. Caputo⁸², R. Cardarelli^{134a}, T. Carli³⁰,
G. Carlino^{103a}, L. Carminati^{90a,90b}, S. Caron¹⁰⁵,
E. Carquin^{32a}, G.D. Carrillo-Montoya^{146c}, J.R. Carter²⁸,
J. Carvalho^{125a,125c}, D. Casadei⁷⁷, M.P. Casado¹²,
M. Casolino¹², E. Castaneda-Miranda^{146b}, A. Castelli¹⁰⁶,
V. Castillo Gimenez¹⁶⁸, N.F. Castro^{125a}, P. Catastini⁵⁷,
A. Catinaccio³⁰, J.R. Catmore¹¹⁸, A. Cattai³⁰,
G. Cattani^{134a,134b}, S. Caughron⁸⁹, V. Cavaliere¹⁶⁶,
D. Cavalli^{90a}, M. Cavalli-Sforza¹², V. Cavasinni^{123a,123b},
F. Ceradini^{135a,135b}, B. Cerio⁴⁵, K. Cerny¹²⁸,
A.S. Cerqueira^{24b}, A. Cerri¹⁵⁰, L. Cerrito⁷⁵, F. Cerutti¹⁵,
M. Cerv³⁰, A. Cervelli¹⁷, S.A. Cetin^{19b}, A. Chafaq^{136a},
D. Chakraborty¹⁰⁷, I. Chalupkova¹²⁸, K. Chan³,
P. Chang¹⁶⁶, B. Chapleau⁸⁶, J.D. Chapman²⁸,
D. Charfeddine¹¹⁶, D.G. Charlton¹⁸, C.C. Chau¹⁵⁹,
C.A. Chavez Barajas¹⁵⁰, S. Cheatham⁸⁶, A. Chegwidden⁸⁹,
S. Chekanov⁶, S.V. Chekulaev^{160a}, G.A. Chelkov⁶⁴,
M.A. Chelstowska⁸⁸, C. Chen⁶³, H. Chen²⁵, K. Chen¹⁴⁹,
L. Chen^{33d,f}, S. Chen^{33c}, X. Chen^{146c}, Y. Chen³⁵,
H.C. Cheng⁸⁸, Y. Cheng³¹, A. Cheplakov⁶⁴,
R. Cherkaoui El Moursli^{136e}, V. Chernyatin^{25,*}, E. Cheu⁷,
L. Chevalier¹³⁷, V. Chiarella⁴⁷, G. Chiefari^{103a,103b},
J.T. Childers⁶, A. Chilingarov⁷¹, G. Chiodini^{72a},
A.S. Chisholm¹⁸, R.T. Chislett⁷⁷, A. Chitan^{26a},
M.V. Chizhov⁶⁴, S. Chouridou⁹, B.K.B. Chow⁹⁹,
I.A. Christidi⁷⁷, D. Chromek-Burckhart³⁰, M.L. Chu¹⁵²,
J. Chudoba¹²⁶, J.J. Chwastowski³⁹, L. Chytka¹¹⁴,
G. Ciapetti^{133a,133b}, A.K. Ciftci^{4a}, R. Ciftci^{4a}, D. Cinca⁶²,
V. Cindro⁷⁴, A. Ciocio¹⁵, P. Cirkovic^{13b}, Z.H. Citron¹⁷³,
M. Citterio^{90a}, M. Ciubancan^{26a}, A. Clark⁴⁹, P.J. Clark⁴⁶,
R.N. Clarke¹⁵, W. Cleland¹²⁴, J.C. Clemens⁸⁴,
C. Clement^{147a,147b}, Y. Coadou⁸⁴, M. Cobal^{165a,165c},
A. Coccaro¹³⁹, J. Cochran⁶³, L. Coffey²³, J.G. Cogan¹⁴⁴,
J. Coggeshall¹⁶⁶, B. Cole³⁵, S. Cole¹⁰⁷, A.P. Colijn¹⁰⁶,
C. Collins-Tooth⁵³, J. Collot⁵⁵, T. Colombo^{58c}, G. Colon⁸⁵,
G. Compostella¹⁰⁰, P. Conde Muñio^{125a,125b},
E. Coniavitis¹⁶⁷, M.C. Conidi¹², S.H. Connell^{146b},
I.A. Connelly⁷⁶, S.M. Consonni^{90a,90b}, V. Consorti⁴⁸,
S. Constantinescu^{26a}, C. Conta^{120a,120b}, G. Conti⁵⁷,
F. Conventi^{103a,g}, M. Cooke¹⁵, B.D. Cooper⁷⁷,
A.M. Cooper-Sarkar¹¹⁹, N.J. Cooper-Smith⁷⁶, K. Copic¹⁵,
T. Cornelissen¹⁷⁶, M. Corradi^{20a}, F. Corrivau^{86,h},
A. Corso-Radu¹⁶⁴, A. Cortes-Gonzalez¹², G. Cortiana¹⁰⁰,
G. Costa^{90a}, M.J. Costa¹⁶⁸, D. Costanzo¹⁴⁰, D. Côté⁸,
G. Cottin²⁸, G. Cowan⁷⁶, B.E. Cox⁸³, K. Cranmer¹⁰⁹,
G. Cree²⁹, S. Crépe-Renaudin⁵⁵, F. Crescioli⁷⁹,
M. Crispin Ortuzar¹¹⁹, M. Cristinziani²¹, V. Croft¹⁰⁵,
G. Crosetti^{37a,37b}, C.-M. Cuciuc^{26a},
T. Cuhadar Donszelmann¹⁴⁰, J. Cummings¹⁷⁷,
M. Curatolo⁴⁷, C. Cuthbert¹⁵¹, H. Cziri¹⁴², P. Czodrowski³,
Z. Czyczula¹⁷⁷, S. D'Auria⁵³, M. D'Onofrio⁷³,
M.J. Da Cunha Sargedas De Sousa^{125a,125b}, C. Da Via⁸³,
W. Dabrowski^{38a}, A. Dafinca¹¹⁹, T. Dai⁸⁸, O. Dale¹⁴,
F. Dallaire⁹⁴, C. Dallapiccola⁸⁵, M. Dam³⁶,
A.C. Daniells¹⁸, M. Dano Hoffmann¹³⁷, V. Dao¹⁰⁵,
G. Darbo^{50a}, G.L. Darlea^{26c}, S. Darmora⁸,
J.A. Dassoulas⁴², A. Dattagupta⁶⁰, W. Davey²¹,
C. David¹⁷⁰, T. Davidek¹²⁸, E. Davies^{119,c}, M. Davies¹⁵⁴,
O. Davignon⁷⁹, A.R. Davison⁷⁷, P. Davison⁷⁷,
Y. Davygora^{58a}, E. Dawe¹⁴³, I. Dawson¹⁴⁰,
R.K. Daya-Ishmukhametova²³, K. De⁸,
R. de Asmundis^{103a}, S. De Castro^{20a,20b}, S. De Cecco⁷⁹,
J. de Graat⁹⁹, N. De Groot¹⁰⁵, P. de Jong¹⁰⁶,
H. De la Torre⁸¹, F. De Lorenzi⁶³, L. De Nooij¹⁰⁶,
D. De Pedis^{133a}, A. De Salvo^{133a}, U. De Sanctis^{165a,165b},
A. De Santo¹⁵⁰, J.B. De Vivie De Regie¹¹⁶,
G. De Zorzi^{133a,133b}, W.J. Dearnaley⁷¹, R. Debbes²⁵,
C. Debenedetti⁴⁶, B. Dechenaux⁵⁵, D.V. Dedovich⁶⁴,
J. Degenhardt¹²¹, I. Deigaard¹⁰⁶, J. Del Peso⁸¹,
T. Del Prete^{123a,123b}, F. Deliot¹³⁷, C.M. Delitzsch⁴⁹,
M. Deliyergiyev⁷⁴, A. Dell'Acqua³⁰, L. Dell'Asta²²,
M. Dell'Orso^{123a,123b}, M. Della Pietra^{103a,g},
D. della Volpe⁴⁹, M. Delmastro⁵, P.A. Delsart⁵⁵,
C. Deluca¹⁰⁶, S. Demers¹⁷⁷, M. Demichev⁶⁴, A. Demilly⁷⁹,
S.P. Denisov¹²⁹, D. Derendarz³⁹, J.E. Derkaoui^{136d},
F. Derue⁷⁹, P. Dervan⁷³, K. Desch²¹, C. Deterre⁴²,
P.O. Deviveiros¹⁰⁶, A. Dewhurst¹³⁰, S. Dhaliwal¹⁰⁶,
A. Di Ciaccio^{134a,134b}, L. Di Ciaccio⁵,
A. Di Domenico^{133a,133b}, C. Di Donato^{103a,103b},
A. Di Girolamo³⁰, B. Di Girolamo³⁰, A. Di Mattia¹⁵³,
B. Di Micco^{135a,135b}, R. Di Nardo⁴⁷, A. Di Simone⁴⁸,
R. Di Sipio^{20a,20b}, D. Di Valentino²⁹, M.A. Diaz^{32a},
E.B. Diehl⁸⁸, J. Dietrich⁴², T.A. Dietzsch^{58a}, S. Diglio⁸⁴,
A. Dimitrievska^{13a}, J. Dingfelder²¹, C. Dionisi^{133a,133b},
P. Dita^{26a}, S. Dita^{26a}, F. Dittus³⁰, F. Djama⁸⁴,
T. Djobava^{51b}, M.A.B. do Vale^{24c},
A. Do Valle Wemans^{125a,125g}, T.K.O. Doan⁵, D. Dobos³⁰,
E. Dobson⁷⁷, C. Dogliani⁴⁹, T. Doherty⁵³, T. Dohmae¹⁵⁶,
J. Dolejsi¹²⁸, Z. Dolezal¹²⁸, B.A. Dolgoshein^{97,*},
M. Donadelli^{24d}, S. Donati^{123a,123b}, P. Dondero^{120a,120b},

J. Donini³⁴, J. Dopke³⁰, A. Doria^{103a}, M.T. Dova⁷⁰,
 A.T. Doyle⁵³, M. Dris¹⁰, J. Dubbert⁸⁸, S. Dube¹⁵,
 E. Dubreuil³⁴, E. Duchovni¹⁷³, G. Duckeck⁹⁹,
 O.A. Ducu^{26a}, D. Duda¹⁷⁶, A. Dudarev³⁰, F. Dudziak⁶³,
 L. Duflog¹¹⁶, L. Duguid⁷⁶, M. Dührssen³⁰, M. Dunford^{58a},
 H. Duran Yildiz^{4a}, M. Düren⁵², A. Durglishvili^{51b},
 M. Dwuznik^{38a}, M. Dyndal^{38a}, J. Ebke⁹⁹, W. Edson²,
 N.C. Edwards⁴⁶, W. Ehrenfeld²¹, T. Eifert¹⁴⁴, G. Eigen¹⁴,
 K. Einsweiler¹⁵, T. Ekelof¹⁶⁷, M. El Kacimi^{136c},
 M. Ellert¹⁶⁷, S. Elles⁵, F. Ellinghaus⁸², N. Ellis³⁰,
 J. Elmsheuser⁹⁹, M. Elsing³⁰, D. Emelianov¹³⁰,
 Y. Enari¹⁵⁶, O.C. Endner⁸², M. Endo¹¹⁷, R. Engelmann¹⁴⁹,
 J. Erdmann¹⁷⁷, A. Ereditato¹⁷, D. Eriksson^{147a}, G. Ernis¹⁷⁶,
 J. Ernst², M. Ernst²⁵, J. Ernwein¹³⁷, D. Errede¹⁶⁶,
 S. Errede¹⁶⁶, E. Ertel⁸², M. Escalier¹¹⁶, H. Esch⁴³,
 C. Escobar¹²⁴, B. Esposito⁴⁷, A.I. Etienvre¹³⁷, E. Etzion¹⁵⁴,
 H. Evans⁶⁰, L. Fabbri^{20a,20b}, G. Facini³⁰,
 R.M. Fakhruddinov¹²⁹, S. Falciano^{133a}, J. Faltova¹²⁸,
 Y. Fang^{33a}, M. Fanti^{90a,90b}, A. Farbin⁸, A. Farilla^{135a},
 T. Farooque¹², S. Farrell¹⁶⁴, S.M. Farrington¹⁷¹,
 P. Farthouat³⁰, F. Fassi¹⁶⁸, P. Fassnacht³⁰, D. Fassouliotis⁹,
 A. Favareto^{50a,50b}, L. Fayard¹¹⁶, P. Federic^{145a},
 O.L. Fedin^{122,i}, W. Fedorko¹⁶⁹, M. Fehling-Kaschek⁴⁸,
 S. Feigl³⁰, L. Feligioni⁸⁴, C. Feng^{33d}, E.J. Feng⁶,
 H. Feng⁸⁸, A.B. Fenyuk¹²⁹, S. Fernandez Perez³⁰,
 S. Ferrag⁵³, J. Ferrando⁵³, A. Ferrari¹⁶⁷, P. Ferrari¹⁰⁶,
 R. Ferrari^{120a}, D.E. Ferreira de Lima⁵³, A. Ferrer¹⁶⁸,
 D. Ferrere⁴⁹, C. Ferretti⁸⁸, A. Ferretto Parodi^{50a,50b},
 M. Fiascaris³¹, F. Fiedler⁸², A. Filipčić⁷⁴, M. Filipuzzi⁴²,
 F. Filthaut¹⁰⁵, M. Fincke-Keeler¹⁷⁰, K.D. Finelli¹⁵¹,
 M.C.N. Fiolhais^{125a,125c}, L. Fiorini¹⁶⁸, A. Firan⁴⁰,
 J. Fischer¹⁷⁶, W.C. Fisher⁸⁹, E.A. Fitzgerald²³, M. Flechl⁴⁸,
 I. Fleck¹⁴², P. Fleischmann¹⁷⁵, S. Fleischmann¹⁷⁶,
 G.T. Fletcher¹⁴⁰, G. Fletcher⁷⁵, T. Flick¹⁷⁶, A. Floderus⁸⁰,
 L.R. Flores Castillo¹⁷⁴, A.C. Florez Bustos^{160b},
 M.J. Flowerdew¹⁰⁰, A. Formica¹³⁷, A. Forti⁸³,
 D. Fortin^{160a}, D. Fournier¹¹⁶, H. Fox⁷¹, S. Fracchia¹²,
 P. Francavilla⁷⁹, M. Franchini^{20a,20b}, S. Franchino³⁰,
 D. Francis³⁰, M. Franklin⁵⁷, S. Franz⁶¹,
 M. Fraternali^{120a,120b}, S.T. French²⁸, C. Friedrich⁴²,
 F. Friedrich⁴⁴, D. Froidevaux³⁰, J.A. Frost²⁸,
 C. Fukunaga¹⁵⁷, E. Fullana Torregrosa⁸², B.G. Fulsom¹⁴⁴,
 J. Fuster¹⁶⁸, C. Gabaldon⁵⁵, O. Gabizon¹⁷³,
 A. Gabrielli^{20a,20b}, A. Gabrielli^{133a,133b}, S. Gadatsch¹⁰⁶,
 S. Gadomski⁴⁹, G. Gagliardi^{50a,50b}, P. Gagnon⁶⁰,
 C. Galea¹⁰⁵, B. Galhardo^{125a,125c}, E.J. Gallas¹¹⁹,
 V. Gallo¹⁷, B.J. Gallop¹³⁰, P. Gallus¹²⁷, G. Galster³⁶,
 K.K. Gan¹¹⁰, R.P. Gandrajula⁶², J. Gao^{33b,f}, Y.S. Gao^{144,e},
 F.M. Garay Walls⁴⁶, F. Garberson¹⁷⁷, C. García¹⁶⁸,
 J.E. García Navarro¹⁶⁸, M. Garcia-Sciveres¹⁵,
 R.W. Gardner³¹, N. Garelli¹⁴⁴, V. Garonne³⁰, C. Gatti⁴⁷,
 G. Gaudio^{120a}, B. Gaur¹⁴², L. Gauthier⁹⁴,
 P. Gauzzi^{133a,133b}, I.L. Gavrilenko⁹⁵, C. Gay¹⁶⁹,
 G. Gaycken²¹, E.N. Gazis¹⁰, P. Ge^{33d}, Z. Gece¹⁶⁹,
 C.N.P. Gee¹³⁰, D.A.A. Geerts¹⁰⁶, Ch. Geich-Gimbel²¹,
 K. Gellerstedt^{147a,147b}, C. Gemme^{50a}, A. Gemmell⁵³,
 M.H. Genest⁵⁵, S. Gentile^{133a,133b}, M. George⁵⁴,
 S. George⁷⁶, D. Gerbaudo¹⁶⁴, A. Gershon¹⁵⁴,
 H. Ghazlane^{136b}, N. Ghodbane³⁴, B. Giacobbe^{20a},
 S. Giagu^{133a,133b}, V. Giangiobbe¹², P. Giannetti^{123a,123b},
 F. Gianotti³⁰, B. Gibbard²⁵, S.M. Gibson⁷⁶,
 M. Gilchriese¹⁵, T.P.S. Gillam²⁸, D. Gillberg³⁰, G. Gilles³⁴,
 D.M. Gingrich^{3,d}, N. Giokaris⁹, M.P. Giordani^{165a,165c},
 R. Giordano^{103a,103b}, F.M. Giorgi¹⁶, P.F. Giraud¹³⁷,
 D. Giugni^{90a}, C. Giuliani⁴⁸, M. Giulini^{58b},
 B.K. Gjelsten¹¹⁸, I. Gkialas^{155,j}, L.K. Gladilin⁹⁸,
 C. Glasman⁸¹, J. Glatzer³⁰, P.C.F. Glaysheer⁴⁶, A. Glazov⁴²,
 G.L. Glonti⁶⁴, M. Goblirsch-Kolb¹⁰⁰, J.R. Goddard⁷⁵,
 J. Godfrey¹⁴³, J. Godlewski³⁰, C. Goeringer⁸²,
 S. Goldfarb⁸⁸, T. Golling¹⁷⁷, D. Golubkov¹²⁹,
 A. Gomes^{125a,125b,125d}, L.S. Gomez Fajardo⁴²,
 R. Gonçalo^{125a}, J. Goncalves Pinto Firmino Da Costa⁴²,
 L. Gonella²¹, S. González de la Hoz¹⁶⁸,
 G. Gonzalez Parra¹², M.L. Gonzalez Silva²⁷,
 S. Gonzalez-Sevilla⁴⁹, L. Goossens³⁰, P.A. Gorbounov⁹⁶,
 H.A. Gordon²⁵, I. Gorelov¹⁰⁴, B. Gorini³⁰, E. Gorini^{72a,72b},
 A. Gorišek⁷⁴, E. Gornicki³⁹, A.T. Goshaw⁶, C. Gössling⁴³,
 M.I. Gostkin⁶⁴, M. Gouighri^{136a}, D. Goujdami^{136c},
 M.P. Goulette⁴⁹, A.G. Goussiou¹³⁹, C. Goy⁵,
 S. Gozpinar²³, H.M.X. Grabas¹³⁷, L. Graber⁵⁴,
 I. Grabowska-Bold^{38a}, P. Grafström^{20a,20b}, K.-J. Grahn⁴²,
 J. Gramling⁴⁹, E. Gramstad¹¹⁸, S. Grancagnolo¹⁶,
 V. Grassi¹⁴⁹, V. Gratchev¹²², H.M. Gray³⁰, E. Graziani^{135a},
 O.G. Grebenyuk¹²², Z.D. Greenwood^{78,k}, K. Gregersen⁷⁷,
 I.M. Gregor⁴², P. Grenier¹⁴⁴, J. Griffiths⁸, A.A. Grillo¹³⁸,
 K. Grimm⁷¹, S. Grinstein^{12,l}, Ph. Gris³⁴,
 Y.V. Grishkevich⁹⁸, J.-F. Grivaz¹¹⁶, J.P. Grohs⁴⁴,
 A. Grohsjean⁴², E. Gross¹⁷³, J. Grosse-Knetter⁵⁴,
 G.C. Grossi^{134a,134b}, J. Groth-Jensen¹⁷³, Z.J. Grout¹⁵⁰,
 K. Grybel¹⁴², L. Guan^{33b}, F. Guescini⁴⁹, D. Guest¹⁷⁷,
 O. Gueta¹⁵⁴, C. Guicheney³⁴, E. Guido^{50a,50b},
 T. Guillemin¹¹⁶, S. Guindon², U. Gul⁵³, C. Gumpert⁴⁴,
 J. Gunther¹²⁷, J. Guo³⁵, S. Gupta¹¹⁹, P. Gutierrez¹¹²,
 N.G. Gutierrez Ortiz⁵³, C. Gutsche⁷⁷, N. Guttman¹⁵⁴,
 C. Guyot¹³⁷, C. Gwenlan¹¹⁹, C.B. Gwilliam⁷³, A. Haas¹⁰⁹,
 C. Haber¹⁵, H.K. Hadavand⁸, N. Haddad^{136e}, P. Haefner²¹,
 S. Hageboeck²¹, Z. Hajduk³⁹, H. Hakobyan¹⁷⁸,
 M. Haleem⁴², D. Hall¹¹⁹, G. Halladjian⁸⁹, K. Hamacher¹⁷⁶,
 P. Hamal¹¹⁴, K. Hamano⁸⁷, M. Hamer⁵⁴, A. Hamilton^{146a},
 S. Hamilton¹⁶², P.G. Hamnett⁴², L. Han^{33b},
 K. Hanagaki¹¹⁷, K. Hanawa¹⁵⁶, M. Hance¹⁵, P. Hanke^{58a},
 J.B. Hansen³⁶, J.D. Hansen³⁶, P.H. Hansen³⁶, K. Hara¹⁶¹,
 A.S. Hard¹⁷⁴, T. Harenberg¹⁷⁶, S. Harkusha⁹¹, D. Harper⁸⁸,
 R.D. Harrington⁴⁶, O.M. Harris¹³⁹, P.F. Harrison¹⁷¹,
 F. Hartjes¹⁰⁶, S. Hasegawa¹⁰², Y. Hasegawa¹⁴¹, A. Hasib¹¹²,
 S. Hassani¹³⁷, S. Haug¹⁷, M. Hauschild³⁰, R. Hauser⁸⁹,

- M. Havranek¹²⁶, C.M. Hawkes¹⁸, R.J. Hawkings³⁰, A.D. Hawkins⁸⁰, T. Hayashi¹⁶¹, D. Hayden⁸⁹, C.P. Hays¹¹⁹, H.S. Hayward⁷³, S.J. Haywood¹³⁰, S.J. Head¹⁸, T. Heck⁸², V. Hedberg⁸⁰, L. Heelan⁸, S. Heim¹²¹, T. Heim¹⁷⁶, B. Heinemann¹⁵, L. Heinrich¹⁰⁹, S. Heisterkamp³⁶, J. Hejbal¹²⁶, L. Helary²², C. Heller⁹⁹, M. Heller³⁰, S. Hellman^{147a,147b}, D. Hellmich²¹, C. Hensens³⁰, J. Henderson¹¹⁹, R.C.W. Henderson⁷¹, C. Hengler⁴², A. Henrichs¹⁷⁷, A.M. Henriques Correia³⁰, S. Henrot-Versille¹¹⁶, C. Hensel⁵⁴, G.H. Herbert¹⁶, Y. Hernández Jiménez¹⁶⁸, R. Herrberg-Schubert¹⁶, G. Herten⁴⁸, R. Hertenberger⁹⁹, L. Hervas³⁰, G.G. Hesketh⁷⁷, N.P. Hesse¹⁰⁶, R. Hickling⁷⁵, E. Higón-Rodríguez¹⁶⁸, E. Hill¹⁷⁰, J.C. Hill²⁸, K.H. Hiller⁴², S. Hillert²¹, S.J. Hillier¹⁸, I. Hinchliffe¹⁵, E. Hines¹²¹, M. Hirose¹¹⁷, D. Hirschbuehl¹⁷⁶, J. Hobbs¹⁴⁹, N. Hod¹⁰⁶, M.C. Hodgkinson¹⁴⁰, P. Hodgson¹⁴⁰, A. Hoecker³⁰, M.R. Hoferkamp¹⁰⁴, J. Hoffman⁴⁰, D. Hoffmann⁸⁴, J.I. Hofmann^{58a}, M. Hohlfeld⁸², T.R. Holmes¹⁵, T.M. Hong¹²¹, L. Hooft van Huysduyenen¹⁰⁹, J.-Y. Hostachy⁵⁵, S. Hou¹⁵², A. Hoummada^{136a}, J. Howard¹¹⁹, J. Howarth⁴², M. Hrabovsky¹¹⁴, I. Hristova¹⁶, J. Hrivnac¹¹⁶, T. Hryn'ova⁵, P.J. Hsu⁸², S.-C. Hsu¹³⁹, D. Hu³⁵, X. Hu²⁵, Y. Huang⁴², Z. Hubacek³⁰, F. Hubaut⁸⁴, F. Huegging²¹, T.B. Huffman¹¹⁹, E.W. Hughes³⁵, G. Hughes⁷¹, M. Huhtinen³⁰, T.A. Hülsing⁸², M. Hurwitz¹⁵, N. Huseynov^{64,b}, J. Huston⁸⁹, J. Huth⁵⁷, G. Iacobucci⁴⁹, G. Iakovidis¹⁰, I. Ibragimov¹⁴², L. Iconomidou-Fayard¹¹⁶, E. Ideal¹⁷⁷, P. Iengo^{103a}, O. Igonkina¹⁰⁶, T. Iizawa¹⁷², Y. Ikegami⁶⁵, K. Ikematsu¹⁴², M. Ikeno⁶⁵, D. Iliadis¹⁵⁵, N. Ilic¹⁵⁹, Y. Inamaru⁶⁶, T. Ince¹⁰⁰, P. Ioannou⁹, M. Iodice^{135a}, K. Iordanidou⁹, V. Ippolito⁵⁷, A. Irlés Quiles¹⁶⁸, C. Isaksson¹⁶⁷, M. Ishino⁶⁷, M. Ishitsuka¹⁵⁸, R. Ishmukhametov¹¹⁰, C. Issever¹¹⁹, S. Istin^{19a}, J.M. Iturbe Ponce⁸³, J. Ivarsson⁸⁰, A.V. Ivashin¹²⁹, W. Iwanski³⁹, H. Iwasaki⁶⁵, J.M. Izen⁴¹, V. Izzo^{103a}, B. Jackson¹²¹, M. Jackson⁷³, P. Jackson¹, M.R. Jaekel³⁰, V. Jain², K. Jakobs⁴⁸, S. Jakobsen³⁰, T. Jakoubek¹²⁶, J. Jakubek¹²⁷, D.O. Jamin¹⁵², D.K. Jana⁷⁸, E. Jansen⁷⁷, H. Jansen³⁰, J. Janssen²¹, M. Janus¹⁷¹, G. Jarlskog⁸⁰, N. Javadov^{64,b}, T. Javůrek⁴⁸, L. Jeanty¹⁵, G.-Y. Jeng¹⁵¹, D. Jennens⁸⁷, P. Jenni^{48,m}, J. Jentsch⁴³, C. Jeske¹⁷¹, S. Jézéquel⁵, H. Ji¹⁷⁴, W. Ji⁸², J. Jia¹⁴⁹, Y. Jiang^{33b}, M. Jimenez Belenguer⁴², S. Jin^{33a}, A. Jinaru^{26a}, O. Jinnouchi¹⁵⁸, M.D. Joergensen³⁶, K.E. Johansson^{147a}, P. Johansson¹⁴⁰, K.A. Johns⁷, K. Jon-And^{147a,147b}, G. Jones¹⁷¹, R.W.L. Jones⁷¹, T.J. Jones⁷³, J. Jongmanns^{58a}, P.M. Jorge^{125a,125b}, K.D. Joshi⁸³, J. Jovicevic¹⁴⁸, X. Ju¹⁷⁴, C.A. Jung⁴³, R.M. Jungst³⁰, P. Jussel⁶¹, A. Juste Rozas^{12,l}, M. Kaci¹⁶⁸, A. Kaczmarska³⁹, M. Kado¹¹⁶, H. Kagan¹¹⁰, M. Kagan¹⁴⁴, E. Kajomovitz⁴⁵, S. Kama⁴⁰, N. Kanaya¹⁵⁶, M. Kaneda³⁰, S. Kaneti²⁸, T. Kanno¹⁵⁸, V.A. Kantserov⁹⁷, J. Kanzaki⁶⁵, B. Kaplan¹⁰⁹, A. Kapliy³¹, D. Kar⁵³, K. Karakostas¹⁰, N. Karastathis¹⁰, M. Karnevskiy⁸², S.N. Karpov⁶⁴, K. Karthik¹⁰⁹, V. Kartvelishvili⁷¹, A.N. Karyukhin¹²⁹, L. Kashif¹⁷⁴, G. Kasieczka^{58b}, R.D. Kass¹¹⁰, A. Kastanas¹⁴, Y. Kataoka¹⁵⁶, A. Katre⁴⁹, J. Katzy⁴², V. Kaushik⁷, K. Kawagoe⁶⁹, T. Kawamoto¹⁵⁶, G. Kawamura⁵⁴, S. Kazama¹⁵⁶, V.F. Kazanin¹⁰⁸, M.Y. Kazarinov⁶⁴, R. Keeler¹⁷⁰, R. Kehoe⁴⁰, M. Keil⁵⁴, J.S. Keller⁴², H. Keoshkerian⁵, O. Kepka¹²⁶, B.P. Kerševan⁷⁴, S. Kersten¹⁷⁶, K. Kessoku¹⁵⁶, J. Keung¹⁵⁹, F. Khalil-zada¹¹, H. Khandanyan^{147a,147b}, A. Khanov¹¹³, A. Khodinov⁹⁷, A. Khomich^{58a}, T.J. Khoo²⁸, G. Khorauli²¹, A. Khoroshilov¹⁷⁶, V. Khovanskiy⁹⁶, E. Khramov⁶⁴, J. Khubua^{51b}, H.Y. Kim⁸, H. Kim^{147a,147b}, S.H. Kim¹⁶¹, N. Kimura¹⁷², O. Kind¹⁶, B.T. King⁷³, M. King¹⁶⁸, R.S.B. King¹¹⁹, S.B. King¹⁶⁹, J. Kirk¹³⁰, A.E. Kiryunin¹⁰⁰, T. Kishimoto⁶⁶, D. Kisielewska^{38a}, F. Kiss⁴⁸, T. Kitamura⁶⁶, T. Kittelmann¹²⁴, K. Kiuchi¹⁶¹, E. Kladiva^{145b}, M. Klein⁷³, U. Klein⁷³, K. Kleinknecht⁸², P. Klimek^{147a,147b}, A. Klimentov²⁵, R. Klingenberg⁴³, J.A. Klinger⁸³, T. Klioutchnikova³⁰, P.F. Klok¹⁰⁵, E.-E. Kluge^{58a}, P. Kluit¹⁰⁶, S. Kluth¹⁰⁰, E. Kneringer⁶¹, E.B.F.G. Knoops⁸⁴, A. Knue⁵³, T. Kobayashi¹⁵⁶, M. Kobel⁴⁴, M. Kocian¹⁴⁴, P. Kodys¹²⁸, P. Koevesarki²¹, T. Koffas²⁹, E. Koffeman¹⁰⁶, L.A. Kogan¹¹⁹, S. Kohlmann¹⁷⁶, Z. Kohout¹²⁷, T. Kohriki⁶⁵, T. Koi¹⁴⁴, H. Kolanoski¹⁶, I. Koletsou⁵, J. Koll⁸⁹, A.A. Komar^{95,*}, Y. Komori¹⁵⁶, T. Kondo⁶⁵, N. Kondrashova⁴², K. Köneke⁴⁸, A.C. König¹⁰⁵, S. König⁸², T. Kono^{65,n}, R. Konoplich^{109,o}, N. Konstantinidis⁷⁷, R. Kopeliansky¹⁵³, S. Koperny^{38a}, L. Köpke⁸², A.K. Kopp⁴⁸, K. Korcyl³⁹, K. Kordas¹⁵⁵, A. Korn⁷⁷, A.A. Korol^{108,p}, I. Korolkov¹², E.V. Korolkova¹⁴⁰, V.A. Korotkov¹²⁹, O. Kortner¹⁰⁰, S. Kortner¹⁰⁰, V.V. Kostyukhin²¹, V.M. Kotov⁶⁴, A. Kotwal⁴⁵, C. Kourkoumelis⁹, V. Kouskoura¹⁵⁵, A. Koutsman^{160a}, R. Kowalewski¹⁷⁰, T.Z. Kowalski^{38a}, W. Kozanecki¹³⁷, A.S. Kozhin¹²⁹, V. Kral¹²⁷, V.A. Kramarenko⁹⁸, G. Kramberger⁷⁴, D. Krasnopevtsev⁹⁷, M.W. Krasny⁷⁹, A. Krasznahorkay³⁰, J.K. Kraus²¹, A. Kravchenko²⁵, S. Kreiss¹⁰⁹, M. Kretz^{58c}, J. Kretzschmar⁷³, K. Kreutzfeldt⁵², P. Krieger¹⁵⁹, K. Kroeninger⁵⁴, H. Kroha¹⁰⁰, J. Kroll¹²¹, J. Kroseberg²¹, J. Krstic^{13a}, U. Kruchonak⁶⁴, H. Krüger²¹, T. Kruker¹⁷, N. Krumnack⁶³, Z.V. Krumshteyn⁶⁴, A. Kruse¹⁷⁴, M.C. Kruse⁴⁵, M. Kruskal²², T. Kubota⁸⁷, S. Kудay^{4a}, S. Kuehn⁴⁸, A. Kugel^{58c}, A. Kuhl¹³⁸, T. Kuhl⁴², V. Kukhtin⁶⁴, Y. Kulchitsky⁹¹, S. Kuleshov^{32b}, M. Kuna^{133a,133b}, J. Kunkle¹²¹, A. Kupco¹²⁶, H. Kurashige⁶⁶, Y.A. Kurochkin⁹¹, R. Kurumida⁶⁶, V. Kus¹²⁶, E.S. Kuwertz¹⁴⁸, M. Kuze¹⁵⁸, J. Kvita¹¹⁴, A. La Rosa⁴⁹, L. La Rotonda^{37a,37b}, C. Lacasta¹⁶⁸, F. Lacava^{133a,133b}, J. Lacey²⁹, H. Lacker¹⁶, D. Lacour⁷⁹, V.R. Lacuesta¹⁶⁸, E. Ladygin⁶⁴, R. Lafaye⁵, B. Laforge⁷⁹,

T. Lagouri¹⁷⁷, S. Lai⁴⁸, H. Laier^{58a}, L. Lambourne⁷⁷,
 S. Lammers⁶⁰, C.L. Lampen⁷, W. Lampl⁷, E. Lançon¹³⁷,
 U. Landgraf⁴⁸, M.P.J. Landon⁷⁵, V.S. Lang^{58a}, C. Lange⁴²,
 A.J. Lankford¹⁶⁴, F. Lanni²⁵, K. Lantzsch³⁰, S. Laplace⁷⁹,
 C. Lapoire²¹, J.F. Laporte¹³⁷, T. Lari^{90a}, M. Lassnig³⁰,
 P. Laurelli⁴⁷, W. Lavrijsen¹⁵, A.T. Law¹³⁸, P. Laycock⁷³,
 B.T. Le⁵⁵, O. Le Dortz⁷⁹, E. Le Guirriec⁸⁴,
 E. Le Menedeu¹², T. LeCompte⁶, F. Ledroit-Guillon⁵⁵,
 C.A. Lee¹⁵², H. Lee¹⁰⁶, J.S.H. Lee¹¹⁷, S.C. Lee¹⁵²,
 L. Lee¹⁷⁷, G. Lefebvre⁷⁹, M. Lefebvre¹⁷⁰, F. Legger⁹⁹,
 C. Leggett¹⁵, A. Lehan⁷³, M. Lehmacher²¹,
 G. Lehmann Miotto³⁰, X. Lei⁷, A.G. Leister¹⁷⁷,
 M.A.L. Leite^{24d}, R. Leitner¹²⁸, D. Lellouch¹⁷³,
 B. Lemmer⁵⁴, K.J.C. Leney⁷⁷, T. Lenz¹⁰⁶, G. Lenzen¹⁷⁶,
 B. Lenzi³⁰, R. Leone⁷, K. Leonhardt⁴⁴, S. Leontsinis¹⁰,
 C. Leroy⁹⁴, C.G. Lester²⁸, C.M. Lester¹²¹,
 M. Levchenko¹²², J. Levêque⁵, D. Levin⁸⁸,
 L.J. Levinson¹⁷³, M. Levy¹⁸, A. Lewis¹¹⁹, G.H. Lewis¹⁰⁹,
 A.M. Leyko²¹, M. Leyton⁴¹, B. Li^{33b,q}, B. Li⁸⁴, H. Li¹⁴⁹,
 H.L. Li³¹, L. Li^{33e}, S. Li⁴⁵, Y. Li^{33c,r}, Z. Liang^{119,s},
 H. Liao³⁴, B. Liberti^{134a}, P. Lichard³⁰, K. Lie¹⁶⁶,
 J. Liebal²¹, W. Liebig¹⁴, C. Limbach²¹, A. Limosani⁸⁷,
 M. Limper⁶², S.C. Lin^{152,t}, F. Linde¹⁰⁶, B.E. Lindquist¹⁴⁹,
 J.T. Linnemann⁸⁹, E. Lipeles¹²¹, A. Lipniacka¹⁴,
 M. Lisovsky⁴², T.M. Liss¹⁶⁶, D. Lissauer²⁵, A. Lister¹⁶⁹,
 A.M. Litke¹³⁸, B. Liu¹⁵², D. Liu¹⁵², J.B. Liu^{33b},
 K. Liu^{33b,u}, L. Liu⁸⁸, M. Liu⁴⁵, M. Liu^{33b}, Y. Liu^{33b},
 M. Livan^{120a,120b}, S.S.A. Livermore¹¹⁹, A. Lleres⁵⁵,
 J. Llorente Merino⁸¹, S.L. Lloyd⁷⁵, F. Lo Sterzo¹⁵²,
 E. Lobodzinska⁴², P. Loch⁷, W.S. Lockman¹³⁸,
 T. Loddenkoetter²¹, F.K. Loebinger⁸³,
 A.E. Loevschall-Jensen³⁶, A. Loginov¹⁷⁷, C.W. Loh¹⁶⁹,
 T. Lohse¹⁶, K. Lohwasser⁴⁸, M. Lokajicek¹²⁶,
 V.P. Lombardo⁵, B.A. Long²², J.D. Long⁸⁸, R.E. Long⁷¹,
 L. Lopes^{125a}, D. Lopez Mateos⁵⁷, B. Lopez Paredes¹⁴⁰,
 J. Lorenz⁹⁹, N. Lorenzo Martinez⁶⁰, M. Losada¹⁶³,
 P. Loscutoff¹⁵, X. Lou⁴¹, A. Lounis¹¹⁶, J. Love⁶,
 P.A. Love⁷¹, A.J. Lowe^{144,e}, F. Lu^{33a}, H.J. Lubatti¹³⁹,
 C. Luci^{133a,133b}, A. Lucotte⁵⁵, F. Luehring⁶⁰, W. Lukas⁶¹,
 L. Luminari^{133a}, O. Lundberg^{147a,147b}, B. Lund-Jensen¹⁴⁸,
 M. Lungwitz⁸², D. Lynn²⁵, R. Lysak¹²⁶, E. Lytken⁸⁰,
 H. Ma²⁵, L.L. Ma^{33d}, G. Maccarrone⁴⁷, A. Macchiolo¹⁰⁰,
 J. Machado Miguens^{125a,125b}, D. Macina³⁰, D. Madaffari⁸⁴,
 R. Madar⁴⁸, H.J. Maddocks⁷¹, W.F. Mader⁴⁴,
 A. Madsen¹⁶⁷, M. Maeno⁸, T. Maeno²⁵, E. Magradze⁵⁴,
 K. Mahboubi⁴⁸, J. Mahlstedt¹⁰⁶, S. Mahmoud⁷³,
 C. Maiani¹³⁷, C. Maidantchik^{24a}, A. Maio^{125a,125b,125d},
 S. Majewski¹¹⁵, Y. Makida⁶⁵, N. Makovec¹¹⁶, P. Mal^{137,v},
 B. Malaescu⁷⁹, Pa. Malecki³⁹, V.P. Maleev¹²², F. Malek⁵⁵,
 U. Mallik⁶², D. Malon⁶, C. Malone¹⁴⁴, S. Maltezos¹⁰,
 V.M. Malyshev¹⁰⁸, S. Malyukov³⁰, J. Mamuzic^{13b},
 B. Mandelli³⁰, L. Mandelli^{90a}, I. Mandić⁷⁴,
 R. Mandrysch⁶², J. Maneira^{125a,125b}, A. Manfredini¹⁰⁰,
 L. Manhaes de Andrade Filho^{24b},
 J.A. Manjarres Ramos^{160b}, A. Mann⁹⁹, P.M. Manning¹³⁸,
 A. Manousakis-Katsikakis⁹, B. Mansoulie¹³⁷,
 R. Mantifel⁸⁶, L. Mapelli³⁰, L. March¹⁶⁸, J.F. Marchand²⁹,
 G. Marchiori⁷⁹, M. Marcisovsky¹²⁶, C.P. Marino¹⁷⁰,
 C.N. Marques^{125a}, F. Marroquim^{24a}, S.P. Marsden⁸³,
 Z. Marshall¹⁵, L.F. Marti¹⁷, S. Marti-Garcia¹⁶⁸,
 B. Martin³⁰, B. Martin⁸⁹, T.A. Martin¹⁷¹, V.J. Martin⁴⁶,
 B. Martin dit Latour¹⁴, H. Martinez¹³⁷, M. Martinez^{12,l},
 S. Martin-Haugh¹³⁰, A.C. Martyniuk⁷⁷, M. Marx¹³⁹,
 F. Marzano^{133a}, A. Marzin³⁰, L. Masetti⁸², T. Mashimo¹⁵⁶,
 R. Mashinistov⁹⁵, J. Masik⁸³, A.L. Maslennikov¹⁰⁸,
 I. Massa^{20a,20b}, N. Massol⁵, P. Mastrandrea¹⁴⁹,
 A. Mastroberardino^{37a,37b}, T. Masubuchi¹⁵⁶,
 H. Matsunaga¹⁵⁶, T. Matsushita⁶⁶, P. Mättig¹⁷⁶,
 S. Mättig⁴², J. Mattmann⁸², J. Maurer^{26a}, S.J. Maxfield⁷³,
 D.A. Maximov^{108,p}, R. Mazini¹⁵², L. Mazzaferro^{134a,134b},
 G. Mc Goldrick¹⁵⁹, S.P. Mc Kee⁸⁸, A. McCarn⁸⁸,
 R.L. McCarthy¹⁴⁹, T.G. McCarthy²⁹, N.A. McCubbin¹³⁰,
 K.W. McFarlane^{56,*}, J.A. McFayden⁷⁷, G. Mchedlize⁵⁴,
 T. McLaughlan¹⁸, S.J. McMahon¹³⁰, R.A. McPherson^{170,h},
 A. Meade⁸⁵, J. Mechnich¹⁰⁶, M. Medinnis⁴², S. Meehan³¹,
 S. Mehlhase³⁶, A. Mehta⁷³, K. Meier^{58a}, C. Meineck⁹⁹,
 B. Meirose⁸⁰, C. Melachrinou³¹, B.R. Mellado Garcia^{146c},
 F. Meloni^{90a,90b}, A. Mengarelli^{20a,20b}, S. Menke¹⁰⁰,
 E. Meoni¹⁶², K.M. Mercurio⁵⁷, S. Mergelmeyer²¹,
 N. Meric¹³⁷, P. Mermod⁴⁹, L. Merola^{103a,103b},
 C. Meroni^{90a}, F.S. Merritt³¹, H. Merritt¹¹⁰, A. Messina^{30,w},
 J. Metcalfe²⁵, A.S. Mete¹⁶⁴, C. Meyer⁸², C. Meyer³¹,
 J-P. Meyer¹³⁷, J. Meyer³⁰, R.P. Middleton¹³⁰, S. Migas⁷³,
 L. Mijović¹³⁷, G. Mikenberg¹⁷³, M. Mikestikova¹²⁶,
 M. Mikuž⁷⁴, D.W. Miller³¹, C. Mills⁴⁶, A. Milov¹⁷³,
 D.A. Milstead^{147a,147b}, D. Milstein¹⁷³, A.A. Minaenko¹²⁹,
 I.A. Minashvili⁶⁴, A.I. Mincer¹⁰⁹, B. Mindur^{38a},
 M. Mineev⁶⁴, Y. Ming¹⁷⁴, L.M. Mir¹², G. Mirabelli^{133a},
 T. Mitani¹⁷², J. Mitrevski⁹⁹, V.A. Mitsou¹⁶⁸, S. Mitsui⁶⁵,
 A. Miucci⁴⁹, P.S. Miyagawa¹⁴⁰, J.U. Mjörnmark⁸⁰,
 T. Moa^{147a,147b}, K. Mochizuki⁸⁴, V. Moeller²⁸,
 S. Mohapatra³⁵, W. Mohr⁴⁸, S. Molander^{147a,147b},
 R. Moles-Valls¹⁶⁸, K. Mönig⁴², C. Monini⁵⁵, J. Monk³⁶,
 E. Monnier⁸⁴, J. Montejo Berlingen¹², F. Monticelli⁷⁰,
 S. Monzani^{133a,133b}, R.W. Moore³, A. Moraes⁵³,
 N. Morange⁶², J. Morel⁵⁴, D. Moreno⁸²,
 M. Moreno Llácer⁵⁴, P. Morettini^{50a}, M. Morgenstern⁴⁴,
 M. Morii⁵⁷, S. Moritz⁸², A.K. Morley¹⁴⁸, G. Mornacchi³⁰,
 J.D. Morris⁷⁵, L. Morvaj¹⁰², H.G. Moser¹⁰⁰,
 M. Mosidze^{51b}, J. Moss¹¹⁰, R. Mount¹⁴⁴, E. Mountricha²⁵,
 S.V. Mouraviev^{95,*}, E.J.W. Moyse⁸⁵, S. Muanza⁸⁴,
 R.D. Mudd¹⁸, F. Mueller^{58a}, J. Mueller¹²⁴, K. Mueller²¹,
 T. Mueller²⁸, T. Mueller⁸², D. Muenstermann⁴⁹,
 Y. Munwes¹⁵⁴, J.A. Murillo Quijada¹⁸, W.J. Murray^{171,130},
 H. Musheghyan⁵⁴, E. Musto¹⁵³, A.G. Myagkov^{129,x},
 M. Myska¹²⁷, O. Nackenhorst⁵⁴, J. Nadal⁵⁴, K. Nagai⁶¹,

- R. Nagai¹⁵⁸, Y. Nagai⁸⁴, K. Nagano⁶⁵, A. Nagarkar¹¹⁰,
Y. Nagasaka⁵⁹, M. Nagel¹⁰⁰, A.M. Nairz³⁰,
Y. Nakahama³⁰, K. Nakamura⁶⁵, T. Nakamura¹⁵⁶,
I. Nakano¹¹¹, H. Namasivayam⁴¹, G. Nanava²¹,
R. Narayan^{58b}, T. Nattermann²¹, T. Naumann⁴²,
G. Navarro¹⁶³, R. Nayyar⁷, H.A. Neal⁸⁸, P.Yu. Nechaeva⁹⁵,
T.J. Neep⁸³, A. Negri^{120a,120b}, G. Negri³⁰, M. Negrini^{20a},
S. Nektarijevic⁴⁹, A. Nelson¹⁶⁴, T.K. Nelson¹⁴⁴,
S. Nemecek¹²⁶, P. Nemethy¹⁰⁹, A.A. Nepomuceno^{24a},
M. Nessi^{30,y}, M.S. Neubauer¹⁶⁶, M. Neumann¹⁷⁶,
R.M. Neves¹⁰⁹, P. Nevski²⁵, P.R. Newman¹⁸,
D.H. Nguyen⁶, R.B. Nickerson¹¹⁹, R. Nicolaidou¹³⁷,
B. Nicquevert³⁰, J. Nielsen¹³⁸, N. Nikiforou³⁵,
A. Nikiforov¹⁶, V. Nikolaenko^{129,x}, I. Nikolic-Audit⁷⁹,
K. Nikolics⁴⁹, K. Nikolopoulos¹⁸, P. Nilsson⁸,
Y. Ninomiya¹⁵⁶, A. Nisati^{133a}, R. Nisius¹⁰⁰, T. Nobe¹⁵⁸,
L. Nodulman⁶, M. Nomachi¹¹⁷, I. Nomidis¹⁵⁵,
S. Norberg¹¹², M. Nordberg³⁰, S. Nowak¹⁰⁰, M. Nozaki⁶⁵,
L. Nozka¹¹⁴, K. Ntekas¹⁰, G. Nunes Hanninger⁸⁷,
T. Nunnemann⁹⁹, E. Nurse⁷⁷, F. Nuti⁸⁷, B.J. O'Brien⁴⁶,
F. O'grady⁷, D.C. O'Neil¹⁴³, V. O'Shea⁵³,
F.G. Oakham^{29,d}, H. Oberlack¹⁰⁰, T. Obermann²¹,
J. Ocariz⁷⁹, A. Ochi⁶⁶, M.I. Ochoa⁷⁷, S. Oda⁶⁹, S. Odaka⁶⁵,
H. Ogren⁶⁰, A. Oh⁸³, S.H. Oh⁴⁵, C.C. Ohm³⁰,
H. Ohman¹⁶⁷, T. Ohshima¹⁰², W. Okamura¹¹⁷, H. Okawa²⁵,
Y. Okumura³¹, T. Okuyama¹⁵⁶, A. Olariu^{26a},
A.G. Olchevski⁶⁴, S.A. Olivares Pino⁴⁶,
D. Oliveira Damazio²⁵, E. Oliver Garcia¹⁶⁸,
A. Olszewski³⁹, J. Olszowska³⁹, A. Onofre^{125a,125e},
P.U.E. Onyisi^{31,z}, C.J. Oram^{160a}, M.J. Oreglia³¹,
Y. Oren¹⁵⁴, D. Orestano^{135a,135b}, N. Orlando^{72a,72b},
C. Oropeza Barrera⁵³, R.S. Orr¹⁵⁹, B. Osculati^{50a,50b},
R. Ospanov¹²¹, G. Otero y Garzon²⁷, H. Otono⁶⁹,
M. Ouchrif^{136d}, E.A. Ouellette¹⁷⁰, F. Ould-Saada¹¹⁸,
A. Ouraou¹³⁷, K.P. Oussoren¹⁰⁶, Q. Ouyang^{33a},
A. Ovcharova¹⁵, M. Owen⁸³, V.E. Ozcan^{19a}, N. Ozturk⁸,
K. Pachal¹¹⁹, A. Pacheco Pages¹², C. Padilla Aranda¹²,
M. Pagáčová⁴⁸, S. Pagan Griso¹⁵, E. Paganis¹⁴⁰, C. Pahl¹⁰⁰,
F. Paige²⁵, P. Pais⁸⁵, K. Pajchel¹¹⁸, G. Palacino^{160b},
S. Palestini³⁰, D. Pallin³⁴, A. Palma^{125a,125b}, J.D. Palmer¹⁸,
Y.B. Pan¹⁷⁴, E. Panagiotopoulou¹⁰,
J.G. Panduro Vazquez⁷⁶, P. Pani¹⁰⁶, N. Panikashvili⁸⁸,
S. Panitkin²⁵, D. Pantea^{26a}, L. Paolozzi^{134a,134b},
Th.D. Papadopoulou¹⁰, K. Papageorgiou^{155,j},
A. Paramonov⁶, D. Paredes Hernandez³⁴, M.A. Parker²⁸,
F. Parodi^{50a,50b}, J.A. Parsons³⁵, U. Parzefall⁴⁸,
E. Pasqualucci^{133a}, S. Passaggio^{50a}, A. Passeri^{135a},
F. Pastore^{135a,135b,*}, Fr. Pastore⁷⁶, G. Pásztor^{49,aa},
S. Patariaia¹⁷⁶, N.D. Patel¹⁵¹, J.R. Pater⁸³,
S. Patricelli^{103a,103b}, T. Pauly³⁰, J. Pearce¹⁷⁰,
M. Pedersen¹¹⁸, S. Pedraza Lopez¹⁶⁸, R. Pedro^{125a,125b},
S.V. Peleganchuk¹⁰⁸, D. Pelikan¹⁶⁷, H. Peng^{33b},
B. Penning³¹, J. Penwell⁶⁰, D.V. Perepelitsa²⁵,
E. Perez Codina^{160a}, M.T. Pérez García-Están¹⁶⁸,
V. Perez Reale³⁵, L. Perini^{90a,90b}, H. Pernegger³⁰,
R. Perrino^{72a}, R. Peschke⁴², V.D. Peshekhonov⁶⁴,
K. Peters³⁰, R.F.Y. Peters⁸³, B.A. Petersen⁸⁷, J. Petersen³⁰,
T.C. Petersen³⁶, E. Petit⁴², A. Petridis^{147a,147b},
C. Petridou¹⁵⁵, E. Petrolo^{133a}, F. Petrucci^{135a,135b},
M. Petteni¹⁴³, N.E. Pettersson¹⁵⁸, R. Pezoa^{32b},
P.W. Phillips¹³⁰, G. Piacquadio¹⁴⁴, E. Pianori¹⁷¹,
A. Picazio⁴⁹, E. Piccaro⁷⁵, M. Piccinini^{20a,20b}, R. Piegaia²⁷,
D.T. Pignotti¹¹⁰, J.E. Pilcher³¹, A.D. Pilkington⁷⁷,
J. Pina^{125a,125b,125d}, M. Pinamonti^{165a,165c,ab}, A. Pinder¹¹⁹,
J.L. Pinfold³, A. Pingel³⁶, B. Pinto^{125a}, S. Pires⁷⁹,
M. Pitt¹⁷³, C. Pizio^{90a,90b}, M.-A. Pleier²⁵, V. Pleskot¹²⁸,
E. Plotnikova⁶⁴, P. Plucinski^{147a,147b}, S. Poddar^{58a},
F. Podlyski³⁴, R. Poettgen⁸², L. Poggioli¹¹⁶, D. Pohl²¹,
M. Pohl⁴⁹, G. Polesello^{120a}, A. Policicchio^{37a,37b},
R. Polifka¹⁵⁹, A. Polini^{20a}, C.S. Pollard⁴⁵,
V. Polychronakos²⁵, K. Pommès³⁰, L. Pontecorvo^{133a},
B.G. Pope⁸⁹, G.A. Popeneciu^{26b}, D.S. Popovic^{13a},
A. Poppleton³⁰, X. Portell Bueso¹², G.E. Pospelov¹⁰⁰,
S. Pospisil¹²⁷, K. Potamianos¹⁵, I.N. Potrap⁶⁴,
C.J. Potter¹⁵⁰, C.T. Potter¹¹⁵, G. Poulard³⁰, J. Poveda⁶⁰,
V. Pozdnyakov⁶⁴, P. Pralavorio⁸⁴, A. Pranko¹⁵, S. Prasad³⁰,
R. Pravahan⁸, S. Prell⁶³, D. Price⁸³, J. Price⁷³, L.E. Price⁶,
D. Prieur¹²⁴, M. Primavera^{72a}, M. Proissl⁴⁶, K. Prokofiev⁴⁷,
F. Prokoshin^{32b}, E. Protopapadaki¹³⁷, S. Protopopescu²⁵,
J. Proudfoot⁶, M. Przybycien^{38a}, H. Przysiezniak⁵,
E. Ptacek¹¹⁵, E. Pueschel⁸⁵, D. Puldon¹⁴⁹, M. Purohit^{25,ac},
P. Puzo¹¹⁶, J. Qian⁸⁸, G. Qin⁵³, Y. Qin⁸³, A. Quadt⁵⁴,
D.R. Quarrie¹⁵, W.B. Quayle^{165a,165b}, D. Quilty⁵³,
A. Qureshi^{160b}, V. Radeka²⁵, V. Radescu⁴²,
S.K. Radhakrishnan¹⁴⁹, P. Radloff¹⁵, P. Rados⁸⁷,
F. Ragusa^{90a,90b}, G. Rahal¹⁷⁹, S. Rajagopalan²⁵,
M. Rammensee³⁰, A.S. Randle-Conde⁴⁰,
C. Rangel-Smith¹⁶⁷, K. Rao¹⁶⁴, F. Rauscher⁹⁹, T.C. Rave⁴⁸,
T. Ravenscroft⁵³, M. Raymond³⁰, A.L. Read¹¹⁸,
D.M. Rebuzzi^{120a,120b}, A. Redelbach¹⁷⁵, G. Redlinger²⁵,
R. Reece¹³⁸, K. Reeves⁴¹, L. Rehnisch¹⁶, A. Reinsch¹¹⁵,
H. Reisin²⁷, M. Relich¹⁶⁴, C. Rembser³⁰, Z.L. Ren¹⁵²,
A. Renaud¹¹⁶, M. Rescigno^{133a}, S. Resconi^{90a},
O.L. Rezanova^{108,p}, P. Reznicek¹²⁸, R. Rezvani⁹⁴,
R. Richter¹⁰⁰, M. Ridel⁷⁹, P. Rieck¹⁶, M. Rijssenbeek¹⁴⁹,
A. Rimoldi^{120a,120b}, L. Rinaldi^{20a}, E. Ritsch⁶¹, I. Riu¹²,
F. Rizatdinova¹¹³, E. Rizvi⁷⁵, S.H. Robertson^{86,h},
A. Robichaud-Veronneau¹¹⁹, D. Robinson²⁸,
J.E.M. Robinson⁸³, A. Robson⁵³, C. Roda^{123a,123b},
L. Rodrigues³⁰, S. Roe³⁰, O. Røhne¹¹⁸, S. Rolli¹⁶²,
A. Romaniouk⁹⁷, M. Romano^{20a,20b}, G. Romeo²⁷,
E. Romero Adam¹⁶⁸, N. Rompotis¹³⁹, L. Roos⁷⁹,
E. Ros¹⁶⁸, S. Rosati^{133a}, K. Rosbach⁴⁹, M. Rose⁷⁶,
P.L. Rosendahl¹⁴, O. Rosenthal¹⁴², V. Rossetti^{147a,147b},
E. Rossi^{103a,103b}, L.P. Rossi^{50a}, R. Rosten¹³⁹, M. Rotaru^{26a},
I. Roth¹⁷³, J. Rothberg¹³⁹, D. Rousseau¹¹⁶, C.R. Royon¹³⁷,

A. Rozanov⁸⁴, Y. Rozen¹⁵³, X. Ruan^{146c}, F. Rubbo¹²,
 I. Rubinskiy⁴², V.I. Rud⁹⁸, C. Rudolph⁴⁴, M.S. Rudolph¹⁵⁹,
 F. Rühr⁴⁸, A. Ruiz-Martinez³⁰, Z. Rurikova⁴⁸,
 N.A. Rusakovich⁶⁴, A. Ruschke⁹⁹, J.P. Rutherford⁷,
 N. Ruthmann⁴⁸, Y.F. Ryabov¹²², M. Rybar¹²⁸,
 G. Rybkin¹¹⁶, N.C. Ryder¹¹⁹, A.F. Saavedra¹⁵¹,
 S. Sacerdoti²⁷, A. Saddique³, I. Sadeh¹⁵⁴,
 H.F.W. Sadrozinski¹³⁸, R. Sadykov⁶⁴, F. Safai Tehrani^{133a},
 H. Sakamoto¹⁵⁶, Y. Sakurai¹⁷², G. Salamanna⁷⁵,
 A. Salamon^{134a}, M. Saleem¹¹², D. Salek¹⁰⁶,
 P.H. Sales De Bruin¹³⁹, D. Salihagic¹⁰⁰, A. Salnikov¹⁴⁴,
 J. Salt¹⁶⁸, B.M. Salvachua Ferrando⁶, D. Salvatore^{37a,37b},
 F. Salvatore¹⁵⁰, A. Salvucci¹⁰⁵, A. Salzburger³⁰,
 D. Sampsonidis¹⁵⁵, A. Sanchez^{103a,103b}, J. Sánchez¹⁶⁸,
 V. Sanchez Martinez¹⁶⁸, H. Sandaker¹⁴, R.L. Sandbach⁷⁵,
 H.G. Sander⁸², M.P. Sanders⁹⁹, M. Sandhoff¹⁷⁶,
 T. Sandoval²⁸, C. Sandoval¹⁶³, R. Sandstroem¹⁰⁰,
 D.P.C. Sankey¹³⁰, A. Sansoni⁴⁷, C. Santoni³⁴,
 R. Santonico^{134a,134b}, H. Santos^{125a}, I. Santoyo Castillo¹⁵⁰,
 K. Sapp¹²⁴, A. Saponov⁶⁴, J.G. Saraiva^{125a,125d},
 B. Sarrazin²¹, G. Sartisohn¹⁷⁶, O. Sasaki⁶⁵, Y. Sasaki¹⁵⁶,
 G. Sauvage^{5,*}, E. Sauvan⁵, P. Savard^{159,d}, D.O. Savu³⁰,
 C. Sawyer¹¹⁹, L. Sawyer^{78,k}, D.H. Saxon⁵³, J. Saxon¹²¹,
 C. Sbarra^{20a}, A. Sbrizzi³, T. Scanlon³⁰,
 D.A. Scannicchio¹⁶⁴, M. Scarcella¹⁵¹, J. Schaarschmidt¹⁷³,
 P. Schacht¹⁰⁰, D. Schaefer¹²¹, R. Schaefer⁴², S. Schaepe²¹,
 S. Schaezel^{58b}, U. Schäfer⁸², A.C. Schaffer¹¹⁶,
 D. Schaile⁹⁹, R.D. Schamberger¹⁴⁹, V. Scharf^{58a},
 V.A. Schegelsky¹²², D. Scheirich¹²⁸, M. Schernau¹⁶⁴,
 M.I. Scherzer³⁵, C. Schiavi^{50a,50b}, J. Schieck⁹⁹,
 C. Schillo⁴⁸, M. Schioppa^{37a,37b}, S. Schlenker³⁰,
 E. Schmidt⁴⁸, K. Schmieden³⁰, C. Schmitt⁸², C. Schmitt⁹⁹,
 S. Schmitt^{58b}, B. Schneider¹⁷, Y.J. Schnellbach⁷³,
 U. Schnoor⁴⁴, L. Schoeffel¹³⁷, A. Schoening^{58b},
 B.D. Schoenrock⁸⁹, A.L.S. Schorlemmer⁵⁴, M. Schott⁸²,
 D. Schouten^{160a}, J. Schovancova²⁵, S. Schramm¹⁵⁹,
 M. Schreyer¹⁷⁵, C. Schroeder⁸², N. Schuh⁸²,
 M.J. Schultens²¹, H.-C. Schultz-Coulon^{58a}, H. Schulz¹⁶,
 M. Schumacher⁴⁸, B.A. Schumm¹³⁸, Ph. Schune¹³⁷,
 A. Schwartzman¹⁴⁴, Ph. Schwegler¹⁰⁰, Ph. Schwemling¹³⁷,
 R. Schwienhorst⁸⁹, J. Schwindling¹³⁷, T. Schwindt²¹,
 M. Schwoerer⁵, F.G. Sciacca¹⁷, E. Scifo¹¹⁶, G. Sciolla²³,
 W.G. Scott¹³⁰, F. Scuri^{123a,123b}, F. Scutti²¹, J. Searcy⁸⁸,
 G. Sedov⁴², E. Sedykh¹²², S.C. Seidel¹⁰⁴, A. Seiden¹³⁸,
 F. Seifert¹²⁷, J.M. Seixas^{24a}, G. Sekhniaidze^{103a},
 S.J. Sekula⁴⁰, K.E. Selbach⁴⁶, D.M. Seliverstov^{122,*},
 G. Sellers⁷³, N. Semprini-Cesari^{20a,20b}, C. Serfon³⁰,
 L. Serin¹¹⁶, L. Serkin⁵⁴, T. Serre⁸⁴, R. Seuster^{160a},
 H. Severini¹¹², F. Sforza¹⁰⁰, A. Sfyrila³⁰, E. Shabalina⁵⁴,
 M. Shamim¹¹⁵, L.Y. Shan^{33a}, J.T. Shank²², Q.T. Shao⁸⁷,
 M. Shapiro¹⁵, P.B. Shatalov⁹⁶, K. Shaw^{165a,165b},
 P. Sherwood⁷⁷, S. Shimizu⁶⁶, C.O. Shimmin¹⁶⁴,
 M. Shimojima¹⁰¹, M. Shiyakova⁶⁴, A. Shmeleva⁹⁵,
 M.J. Shochet³¹, D. Short¹¹⁹, S. Shrestha⁶³, E. Shulga⁹⁷,
 M.A. Shupe⁷, S. Shushkevich⁴², P. Sicho¹²⁶, D. Sidorov¹¹³,
 A. Sidoti^{133a}, F. Siegert⁴⁴, Dj. Sijacki^{13a}, O. Silbert¹⁷³,
 J. Silva^{125a,125d}, Y. Silver¹⁵⁴, D. Silverstein¹⁴⁴,
 S.B. Silverstein^{147a}, V. Simak¹²⁷, O. Simard⁵, Lj. Simic^{13a},
 S. Simion¹¹⁶, E. Simioni⁸², B. Simmons⁷⁷,
 R. Simoniello^{90a,90b}, M. Simonyan³⁶, P. Sinervo¹⁵⁹,
 N.B. Sinev¹¹⁵, V. Sipica¹⁴², G. Siragusa¹⁷⁵, A. Sircar⁷⁸,
 A.N. Sisakyan^{64,*}, S.Yu. Sivoklokov⁹⁸, J. Sjölin^{147a,147b},
 T.B. Sjusen¹⁴, H.P. Skottowe⁵⁷, K. Yu. Skovpen¹⁰⁸,
 P. Skubic¹¹², M. Slater¹⁸, T. Slavicek¹²⁷, K. Sliwa¹⁶²,
 V. Smakhtin¹⁷³, B.H. Smart⁴⁶, L. Smestad¹⁴,
 S.Yu. Smirnov⁹⁷, Y. Smirnov⁹⁷, L.N. Smirnova^{98,ad},
 O. Smirnova⁸⁰, K.M. Smith⁵³, M. Smizanska⁷¹,
 K. Smolek¹²⁷, A.A. Snesarev⁹⁵, G. Snidero⁷⁵, S. Snyder²⁵,
 R. Sobie^{170,h}, F. Socher⁴⁴, A. Soffer¹⁵⁴, D.A. Soh^{152,s},
 C.A. Solans³⁰, M. Solar¹²⁷, J. Solc¹²⁷, E.Yu. Soldatov⁹⁷,
 U. Soldevila¹⁶⁸, E. Solfaroli Camillocci^{133a,133b},
 A.A. Solodkov¹²⁹, O.V. Solovyanov¹²⁹, V. Solovyev¹²²,
 P. Sommer⁴⁸, H.Y. Song^{33b}, N. Soni¹, A. Sood¹⁵,
 A. Sopczak¹²⁷, V. Sopko¹²⁷, B. Sopko¹²⁷, V. Sorin¹²,
 M. Sosebee⁸, R. Soualah^{165a,165c}, P. Soueid⁹⁴,
 A.M. Soukharev¹⁰⁸, D. South⁴², S. Spagnolo^{72a,72b},
 F. Spanò⁷⁶, W.R. Spearman⁵⁷, R. Spighi^{20a}, G. Spigo³⁰,
 M. Spousta¹²⁸, T. Spreitzer¹⁵⁹, B. Spurlock⁸,
 R.D. St. Denis⁵³, S. Staerz⁴⁴, J. Stahlman¹²¹, R. Stamen^{58a},
 E. Stanecka³⁹, R.W. Stanek⁶, C. Stanescu^{135a},
 M. Stanescu-Bellu⁴², M.M. Stanitzki⁴², S. Stapnes¹¹⁸,
 E.A. Starchenko¹²⁹, J. Stark⁵⁵, P. Staroba¹²⁶,
 P. Starovoitov⁴², R. Staszewski³⁹, P. Stavina^{145a,*},
 G. Steele⁵³, P. Steinberg²⁵, B. Stelzer¹⁴³, H.J. Stelzer³⁰,
 O. Stelzer-Chilton^{160a}, H. Stenzel⁵², S. Stern¹⁰⁰,
 G.A. Stewart⁵³, J.A. Stillings²¹, M.C. Stockton⁸⁶,
 M. Stoebe⁸⁶, G. Stoicea^{26a}, P. Stolte⁵⁴, S. Stonjek¹⁰⁰,
 A.R. Stradling⁸, A. Straessner⁴⁴, M.E. Stramaglia¹⁷,
 J. Strandberg¹⁴⁸, S. Strandberg^{147a,147b}, A. Strandlie¹¹⁸,
 E. Strauss¹⁴⁴, M. Strauss¹¹², P. Strizenec^{145b},
 R. Ströhmer¹⁷⁵, D.M. Strom¹¹⁵, R. Stroynowski⁴⁰,
 S.A. Stucci¹⁷, B. Stugu¹⁴, N.A. Styles⁴², D. Su¹⁴⁴, J. Su¹²⁴,
 HS. Subramania³, R. Subramaniam⁷⁸, A. Succurro¹²,
 Y. Sugaya¹¹⁷, C. Suhr¹⁰⁷, M. Suk¹²⁷, V.V. Sulin⁹⁵,
 S. Sultansoy^{4c}, T. Sumida⁶⁷, X. Sun^{33a}, J.E. Sundermann⁴⁸,
 K. Suruliz¹⁴⁰, G. Susinno^{37a,37b}, M.R. Sutton¹⁵⁰,
 Y. Suzuki⁶⁵, M. Svatos¹²⁶, S. Swedish¹⁶⁹,
 M. Swiatlowski¹⁴⁴, I. Sykora^{145a}, T. Sykora¹²⁸, D. Ta⁸⁹,
 K. Tackmann⁴², J. Taenzer¹⁵⁹, A. Taffard¹⁶⁴,
 R. Tafirot^{160a}, N. Taiblum¹⁵⁴, Y. Takahashi¹⁰², H. Takai²⁵,
 R. Takashima⁶⁸, H. Takeda⁶⁶, T. Takeshita¹⁴¹, Y. Takubo⁶⁵,
 M. Talby⁸⁴, A.A. Talyshv^{108,p}, J.Y.C. Tam¹⁷⁵,
 M.C. Tamsett^{78,ae}, K.G. Tan⁸⁷, J. Tanaka¹⁵⁶, R. Tanaka¹¹⁶,
 S. Tanaka¹³², S. Tanaka⁶⁵, A.J. Tanasijczuk¹⁴³, K. Tani⁶⁶,
 N. Tannoury⁸⁴, S. Tapprogge⁸², S. Tarem¹⁵³, F. Tarrade²⁹,
 G.F. Tartarelli^{90a}, P. Tas¹²⁸, M. Tasevsky¹²⁶, T. Tashiro⁶⁷,

- E. Tassi^{37a,37b}, A. Tavares Delgado^{125a,125b}, Y. Tayalati^{136d}, F.E. Taylor⁹³, G.N. Taylor⁸⁷, W. Taylor^{160b}, F.A. Teischinger³⁰, M. Teixeira Dias Castanheira⁷⁵, P. Teixeira-Dias⁷⁶, K.K. Temming⁴⁸, H. Ten Kate³⁰, P.K. Teng¹⁵², S. Terada⁶⁵, K. Terashi¹⁵⁶, J. Terron⁸¹, S. Terzo¹⁰⁰, M. Testa⁴⁷, R.J. Teuscher^{159,h}, J. Therhaag²¹, T. Theveneaux-Pelzer³⁴, S. Thoma⁴⁸, J.P. Thomas¹⁸, J. Thomas-Wilsker⁷⁶, E.N. Thompson³⁵, P.D. Thompson¹⁸, P.D. Thompson¹⁵⁹, A.S. Thompson⁵³, L.A. Thomsen³⁶, E. Thomson¹²¹, M. Thomson²⁸, W.M. Thong⁸⁷, R.P. Thun^{88,*}, F. Tian³⁵, M.J. Tibbetts¹⁵, V.O. Tikhomirov^{95.af}, Yu.A. Tikhonov^{108.p}, S. Timoshenko⁹⁷, E. Tiouchichine⁸⁴, P. Tipton¹⁷⁷, S. Tisserant⁸⁴, T. Todorov⁵, S. Todorova-Nova¹²⁸, B. Toggerson⁷, J. Tojo⁶⁹, S. Tokár^{145a}, K. Tokushuku⁶⁵, K. Tollefson⁸⁹, L. Tomlinson⁸³, M. Tomoto¹⁰², L. Tompkins³¹, K. Toms¹⁰⁴, N.D. Topilin⁶⁴, E. Torrence¹¹⁵, H. Torres¹⁴³, E. Torró Pastor¹⁶⁸, J. Toth^{84.aa}, F. Touchard⁸⁴, D.R. Tovey¹⁴⁰, H.L. Tran¹¹⁶, T. Trefzger¹⁷⁵, L. Tremblet³⁰, A. Tricoli³⁰, I.M. Trigger^{160a}, S. Trincaz-Duvoid⁷⁹, M.F. Tripiana⁷⁰, N. Triplett²⁵, W. Trischuk¹⁵⁹, B. Trocmé⁵⁵, C. Troncon^{90a}, M. Trotter-McDonald¹⁴³, M. Trovatelli^{135a,135b}, P. True⁸⁹, M. Trzebinski³⁹, A. Trzupek³⁹, C. Tsarouchas³⁰, J.C.-L. Tseng¹¹⁹, P.V. Tsiarshka⁹¹, D. Tsiou¹³⁷, G. Tsipolitis¹⁰, N. Tsirintanis⁹, S. Tsiskaridze¹², V. Tsiskaridze⁴⁸, E.G. Tskhadadze^{51a}, I.I. Tsukerman⁹⁶, V. Tsulaia¹⁵, S. Tsuno⁶⁵, D. Tsybychev¹⁴⁹, A. Tudorache^{26a}, V. Tudorache^{26a}, A.N. Tuna¹²¹, S.A. Tuppuri^{20a,20b}, S. Turchikhin^{98.ad}, D. Turecek¹²⁷, I. Turk Cakir^{4d}, R. Turra^{90a,90b}, P.M. Tuts³⁵, A. Tykhonov⁷⁴, M. Tylmad^{147a,147b}, M. Tyndel¹³⁰, K. Uchida²¹, I. Ueda¹⁵⁶, R. Ueno²⁹, M. Ughetto⁸⁴, M. Uglund¹⁴, M. Uhlenbrock²¹, F. Ukegawa¹⁶¹, G. Unal³⁰, A. Undrus²⁵, G. Unel¹⁶⁴, F.C. Ungaro⁴⁸, Y. Unno⁶⁵, D. Urbaniec³⁵, P. Urquijo²¹, G. Usai⁸, A. Usanova⁶¹, L. Vacavant⁸⁴, V. Vacek¹²⁷, B. Vachon⁸⁶, N. Valencic¹⁰⁶, S. Valentini^{20a,20b}, A. Valero¹⁶⁸, L. Valery³⁴, S. Valkar¹²⁸, E. Valladolid Gallego¹⁶⁸, S. Vallecorsa⁴⁹, J.A. Valls Ferrer¹⁶⁸, P.C. Van Der Deijl¹⁰⁶, R. van der Geer¹⁰⁶, H. van der Graaf¹⁰⁶, R. Van Der Leeuw¹⁰⁶, D. van der Ster³⁰, N. van Eldik³⁰, P. van Gemmeren⁶, J. Van Nieuwkoop¹⁴³, I. van Vulpen¹⁰⁶, M.C. van Woerden³⁰, M. Vanadia^{133a,133b}, W. Vandelli³⁰, R. Vanguri¹²¹, A. Vaniachine⁶, P. Vankov⁴², F. Vannucci⁷⁹, G. Vardanyan¹⁷⁸, R. Vari^{133a}, E.W. Varnes⁷, T. Varol⁸⁵, D. Varouchas⁷⁹, A. Vartapetian⁸, K.E. Varvell¹⁵¹, F. Vazeille³⁴, T. Vazquez Schroeder⁵⁴, J. Veatch⁷, F. Veloso^{125a,125c}, S. Veneziano^{133a}, A. Ventura^{72a,72b}, D. Ventura⁸⁵, M. Venturi⁴⁸, N. Venturi¹⁵⁹, A. Venturini²³, V. Vercesi^{120a}, M. Verducci¹³⁹, W. Verkerke¹⁰⁶, J.C. Vermeulen¹⁰⁶, A. Vest⁴⁴, M.C. Vetterli^{143.d}, O. Viazlo⁸⁰, I. Vichou¹⁶⁶, T. Vickey^{146c.ag}, O.E. Vickey Boeriu^{146c}, G.H.A. Viehhauser¹¹⁹, S. Viel¹⁶⁹, R. Vigne³⁰, M. Villa^{20a,20b}, M. Villaplana Perez¹⁶⁸, E. Vilucchi⁴⁷, M.G. Vincker²⁹, V.B. Vinogradov⁶⁴, J. Virzi¹⁵, I. Vivarelli¹⁵⁰, F. Vives Vaque³, S. Vlachos¹⁰, D. Vladioiu⁹⁹, M. Vlasak¹²⁷, A. Vogel²¹, P. Vokac¹²⁷, G. Volpi^{123a,123b}, M. Volpi⁸⁷, H. von der Schmitt¹⁰⁰, H. von Radziewski⁴⁸, E. von Toerne²¹, V. Vorobel¹²⁸, K. Vorobev⁹⁷, M. Vos¹⁶⁸, R. Voss³⁰, J.H. Vosseveld⁷³, N. Vranjes¹³⁷, M. Vranjes Milosavljevic¹⁰⁶, V. Vrba¹²⁶, M. Vreeswijk¹⁰⁶, T. Vu Anh⁴⁸, R. Vuillermet³⁰, I. Vukotic³¹, Z. Vykydal¹²⁷, W. Wagner¹⁷⁶, P. Wagner²¹, S. Wahrmund⁴⁴, J. Wakabayashi¹⁰², J. Walder⁷¹, R. Walker⁹⁹, W. Walkowiak¹⁴², R. Wall¹⁷⁷, P. Waller⁷³, B. Walsh¹⁷⁷, C. Wang^{152.ah}, C. Wang⁴⁵, F. Wang¹⁷⁴, H. Wang¹⁵, H. Wang⁴⁰, J. Wang⁴², J. Wang^{33a}, K. Wang⁸⁶, R. Wang¹⁰⁴, S.M. Wang¹⁵², T. Wang²¹, X. Wang¹⁷⁷, C. Wanotayaroj¹¹⁵, A. Warburton⁸⁶, C.P. Ward²⁸, D.R. Wardrope⁷⁷, M. Warsinsky⁴⁸, A. Washbrook⁴⁶, C. Wasicki⁴², I. Watanabe⁶⁶, P.M. Watkins¹⁸, A.T. Watson¹⁸, I.J. Watson¹⁵¹, M.F. Watson¹⁸, G. Watts¹³⁹, S. Watts⁸³, B.M. Waugh⁷⁷, S. Webb⁸³, M.S. Weber¹⁷, S.W. Weber¹⁷⁵, J.S. Webster³¹, A.R. Weidberg¹¹⁹, P. Weigell¹⁰⁰, B. Weinert⁶⁰, J. Weingarten⁵⁴, C. Weiser⁴⁸, H. Weits¹⁰⁶, P.S. Wells³⁰, T. Wenaus²⁵, D. Wendland¹⁶, Z. Weng^{152.s}, T. Wengler³⁰, S. Wenig³⁰, N. Wermes²¹, M. Werner⁴⁸, P. Werner³⁰, M. Wessels^{58a}, J. Wetter¹⁶², K. Whalen²⁹, A. White⁸, M.J. White¹, R. White^{32b}, S. White^{123a,123b}, D. Whiteson¹⁶⁴, D. Wicke¹⁷⁶, F.J. Wickens¹³⁰, W. Wiedenmann¹⁷⁴, M. Wielers¹³⁰, P. Wienemann²¹, C. Wiglesworth³⁶, L.A.M. Wiik-Fuchs²¹, P.A. Wijeratne⁷⁷, A. Wildauer¹⁰⁰, M.A. Wildt^{42.ai}, H.G. Wilkens³⁰, J.Z. Will⁹⁹, H.H. Williams¹²¹, S. Williams²⁸, C. Willis⁸⁹, S. Willocq⁸⁵, J.A. Wilson¹⁸, A. Wilson⁸⁸, I. Wingerter-Seez⁵, F. Winklmeier¹¹⁵, M. Wittgen¹⁴⁴, T. Wittig⁴³, J. Wittkowski⁹⁹, S.J. Wollstadt⁸², M.W. Wolter³⁹, H. Wolters^{125a,125c}, B.K. Wosiek³⁹, J. Wotschack³⁰, M.J. Woudstra⁸³, K.W. Wozniak³⁹, M. Wright⁵³, M. Wu⁵⁵, S.L. Wu¹⁷⁴, X. Wu⁴⁹, Y. Wu⁸⁸, E. Wulf³⁵, T.R. Wyatt⁸³, B.M. Wynne⁴⁶, S. Xella³⁶, M. Xiao¹³⁷, D. Xu^{33a}, L. Xu^{33b.aj}, B. Yabsley¹⁵¹, S. Yacoob^{146b.ak}, M. Yamada⁶⁵, H. Yamaguchi¹⁵⁶, Y. Yamaguchi¹⁵⁶, A. Yamamoto⁶⁵, K. Yamamoto⁶³, S. Yamamoto¹⁵⁶, T. Yamamura¹⁵⁶, T. Yamanaka¹⁵⁶, K. Yamauchi¹⁰², Y. Yamazaki⁶⁶, Z. Yan²², H. Yang^{33e}, H. Yang¹⁷⁴, U.K. Yang⁸³, Y. Yang¹¹⁰, S. Yanush⁹², L. Yao^{33a}, W.-M. Yao¹⁵, Y. Yasu⁶⁵, E. Yatsenko⁴², K.H. Yau Wong²¹, J. Ye⁴⁰, S. Ye²⁵, A.L. Yen⁵⁷, E. Yildirim⁴², M. Yilmaz^{4b}, R. Yoosoofmiya¹²⁴, K. Yorita¹⁷², R. Yoshida⁶, K. Yoshihara¹⁵⁶, C. Young¹⁴⁴, C.J.S. Young³⁰, S. Youssef²², D.R. Yu¹⁵, J. Yu⁸, J.M. Yu⁸⁸, J. Yu¹¹³, L. Yuan⁶⁶, A. Yurkewicz¹⁰⁷, B. Zabinski³⁹, R. Zaidan⁶², A.M. Zaitsev^{129.x}, A. Zaman¹⁴⁹, S. Zambito²³,

L. Zanello^{133a,133b}, D. Zanzi¹⁰⁰, A. Zaytsev²⁵,
 C. Zeitnitz¹⁷⁶, M. Zeman¹²⁷, A. Zemla^{38a}, K. Zengel²³,
 O. Zenin¹²⁹, T. Ženiš^{145a}, D. Zerwas¹¹⁶,
 G. Zevi della Porta⁵⁷, D. Zhang⁸⁸, F. Zhang¹⁷⁴, H. Zhang⁸⁹,
 J. Zhang⁶, L. Zhang¹⁵², X. Zhang^{33d}, Z. Zhang¹¹⁶,
 Z. Zhao^{33b}, A. Zhemchugov⁶⁴, J. Zhong¹¹⁹, B. Zhou⁸⁸,
 L. Zhou³⁵, N. Zhou¹⁶⁴, C.G. Zhu^{33d}, H. Zhu^{33a}, J. Zhu⁸⁸,
 Y. Zhu^{33b}, X. Zhuang^{33a}, A. Zibell¹⁷⁵, D. Zieminska⁶⁰,
 N.I. Zimine⁶⁴, C. Zimmermann⁸², R. Zimmermann²¹,
 S. Zimmermann²¹, S. Zimmermann⁴⁸, Z. Zinonos⁵⁴,
 M. Ziolkowski¹⁴², G. Zobernig¹⁷⁴, A. Zoccoli^{20a,20b},
 M. zur Nedden¹⁶, G. Zurzolo^{103a,103b}, V. Zutshi¹⁰⁷,
 L. Zwalinski³⁰.

¹ Department of Physics, University of Adelaide, Adelaide, Australia

² Physics Department, SUNY Albany, Albany NY, United States of America

³ Department of Physics, University of Alberta, Edmonton AB, Canada

⁴ (a) Department of Physics, Ankara University, Ankara; (b) Department of Physics, Gazi University, Ankara; (c) Division of Physics, TOBB University of Economics and Technology, Ankara; (d) Turkish Atomic Energy Authority, Ankara, Turkey

⁵ LAPP, CNRS/IN2P3 and Université de Savoie, Annecy-le-Vieux, France

⁶ High Energy Physics Division, Argonne National Laboratory, Argonne IL, United States of America

⁷ Department of Physics, University of Arizona, Tucson AZ, United States of America

⁸ Department of Physics, The University of Texas at Arlington, Arlington TX, United States of America

⁹ Physics Department, University of Athens, Athens, Greece

¹⁰ Physics Department, National Technical University of Athens, Zografou, Greece

¹¹ Institute of Physics, Azerbaijan Academy of Sciences, Baku, Azerbaijan

¹² Institut de Física d'Altes Energies and Departament de Física de la Universitat Autònoma de Barcelona, Barcelona, Spain

¹³ (a) Institute of Physics, University of Belgrade, Belgrade; (b) Vinca Institute of Nuclear Sciences, University of Belgrade, Belgrade, Serbia

¹⁴ Department for Physics and Technology, University of Bergen, Bergen, Norway

¹⁵ Physics Division, Lawrence Berkeley National Laboratory and University of California, Berkeley CA, United States of America

¹⁶ Department of Physics, Humboldt University, Berlin, Germany

¹⁷ Albert Einstein Center for Fundamental Physics and Laboratory for High Energy Physics, University of Bern, Bern, Switzerland

¹⁸ School of Physics and Astronomy, University of Birmingham, Birmingham, United Kingdom

¹⁹ (a) Department of Physics, Bogazici University, Istanbul;

(b) Department of Physics, Dogus University, Istanbul; (c)

Department of Physics Engineering, Gaziantep University, Gaziantep, Turkey

²⁰ (a) INFN Sezione di Bologna; (b) Dipartimento di Fisica e Astronomia, Università di Bologna, Bologna, Italy

²¹ Physikalisches Institut, University of Bonn, Bonn, Germany

²² Department of Physics, Boston University, Boston MA, United States of America

²³ Department of Physics, Brandeis University, Waltham MA, United States of America

²⁴ (a) Universidade Federal do Rio De Janeiro

COPPE/EE/IF, Rio de Janeiro; (b) Federal University of Juiz de Fora (UFJF), Juiz de Fora; (c) Federal University of Sao Joao del Rei (UFSJ), Sao Joao del Rei; (d) Instituto de Física, Universidade de Sao Paulo, Sao Paulo, Brazil

²⁵ Physics Department, Brookhaven National Laboratory, Upton NY, United States of America

²⁶ (a) National Institute of Physics and Nuclear Engineering, Bucharest; (b) National Institute for Research and Development of Isotopic and Molecular Technologies, Physics Department, Cluj Napoca; (c) University Politehnica Bucharest, Bucharest; (d) West University in Timisoara, Timisoara, Romania

²⁷ Departamento de Física, Universidad de Buenos Aires, Buenos Aires, Argentina

²⁸ Cavendish Laboratory, University of Cambridge, Cambridge, United Kingdom

²⁹ Department of Physics, Carleton University, Ottawa ON, Canada

³⁰ CERN, Geneva, Switzerland

³¹ Enrico Fermi Institute, University of Chicago, Chicago IL, United States of America

³² (a) Departamento de Física, Pontificia Universidad Católica de Chile, Santiago; (b) Departamento de Física, Universidad Técnica Federico Santa María, Valparaíso, Chile

³³ (a) Institute of High Energy Physics, Chinese Academy of Sciences, Beijing; (b) Department of Modern Physics, University of Science and Technology of China, Anhui; (c) Department of Physics, Nanjing University, Jiangsu; (d) School of Physics, Shandong University, Shandong; (e) Physics Department, Shanghai Jiao Tong University, Shanghai, China

³⁴ Laboratoire de Physique Corpusculaire, Clermont Université and Université Blaise Pascal and CNRS/IN2P3, Clermont-Ferrand, France

- ³⁵ Nevis Laboratory, Columbia University, Irvington NY, United States of America
- ³⁶ Niels Bohr Institute, University of Copenhagen, Copenhagen, Denmark
- ³⁷ ^(a) INFN Gruppo Collegato di Cosenza, Laboratori Nazionali di Frascati; ^(b) Dipartimento di Fisica, Università della Calabria, Rende, Italy
- ³⁸ ^(a) AGH University of Science and Technology, Faculty of Physics and Applied Computer Science, Krakow; ^(b) Marian Smoluchowski Institute of Physics, Jagiellonian University, Krakow, Poland
- ³⁹ The Henryk Niewodniczanski Institute of Nuclear Physics, Polish Academy of Sciences, Krakow, Poland
- ⁴⁰ Physics Department, Southern Methodist University, Dallas TX, United States of America
- ⁴¹ Physics Department, University of Texas at Dallas, Richardson TX, United States of America
- ⁴² DESY, Hamburg and Zeuthen, Germany
- ⁴³ Institut für Experimentelle Physik IV, Technische Universität Dortmund, Dortmund, Germany
- ⁴⁴ Institut für Kern- und Teilchenphysik, Technische Universität Dresden, Dresden, Germany
- ⁴⁵ Department of Physics, Duke University, Durham NC, United States of America
- ⁴⁶ SUPA - School of Physics and Astronomy, University of Edinburgh, Edinburgh, United Kingdom
- ⁴⁷ INFN Laboratori Nazionali di Frascati, Frascati, Italy
- ⁴⁸ Fakultät für Mathematik und Physik, Albert-Ludwigs-Universität, Freiburg, Germany
- ⁴⁹ Section de Physique, Université de Genève, Geneva, Switzerland
- ⁵⁰ ^(a) INFN Sezione di Genova; ^(b) Dipartimento di Fisica, Università di Genova, Genova, Italy
- ⁵¹ ^(a) E. Andronikashvili Institute of Physics, Iv. Javakishvili Tbilisi State University, Tbilisi; ^(b) High Energy Physics Institute, Tbilisi State University, Tbilisi, Georgia
- ⁵² II Physikalisches Institut, Justus-Liebig-Universität Giessen, Giessen, Germany
- ⁵³ SUPA - School of Physics and Astronomy, University of Glasgow, Glasgow, United Kingdom
- ⁵⁴ II Physikalisches Institut, Georg-August-Universität, Göttingen, Germany
- ⁵⁵ Laboratoire de Physique Subatomique et de Cosmologie, Université Grenoble-Alpes, CNRS/IN2P3, Grenoble, France
- ⁵⁶ Department of Physics, Hampton University, Hampton VA, United States of America
- ⁵⁷ Laboratory for Particle Physics and Cosmology, Harvard University, Cambridge MA, United States of America
- ⁵⁸ ^(a) Kirchhoff-Institut für Physik, Ruprecht-Karls-Universität Heidelberg, Heidelberg; ^(b) Physikalisches Institut, Ruprecht-Karls-Universität Heidelberg, Heidelberg; ^(c) ZITI Institut für technische Informatik, Ruprecht-Karls-Universität Heidelberg, Mannheim, Germany
- ⁵⁹ Faculty of Applied Information Science, Hiroshima Institute of Technology, Hiroshima, Japan
- ⁶⁰ Department of Physics, Indiana University, Bloomington IN, United States of America
- ⁶¹ Institut für Astro- und Teilchenphysik, Leopold-Franzens-Universität, Innsbruck, Austria
- ⁶² University of Iowa, Iowa City IA, United States of America
- ⁶³ Department of Physics and Astronomy, Iowa State University, Ames IA, United States of America
- ⁶⁴ Joint Institute for Nuclear Research, JINR Dubna, Dubna, Russia
- ⁶⁵ KEK, High Energy Accelerator Research Organization, Tsukuba, Japan
- ⁶⁶ Graduate School of Science, Kobe University, Kobe, Japan
- ⁶⁷ Faculty of Science, Kyoto University, Kyoto, Japan
- ⁶⁸ Kyoto University of Education, Kyoto, Japan
- ⁶⁹ Department of Physics, Kyushu University, Fukuoka, Japan
- ⁷⁰ Instituto de Física La Plata, Universidad Nacional de La Plata and CONICET, La Plata, Argentina
- ⁷¹ Physics Department, Lancaster University, Lancaster, United Kingdom
- ⁷² ^(a) INFN Sezione di Lecce; ^(b) Dipartimento di Matematica e Fisica, Università del Salento, Lecce, Italy
- ⁷³ Oliver Lodge Laboratory, University of Liverpool, Liverpool, United Kingdom
- ⁷⁴ Department of Physics, Jožef Stefan Institute and University of Ljubljana, Ljubljana, Slovenia
- ⁷⁵ School of Physics and Astronomy, Queen Mary University of London, London, United Kingdom
- ⁷⁶ Department of Physics, Royal Holloway University of London, Surrey, United Kingdom
- ⁷⁷ Department of Physics and Astronomy, University College London, London, United Kingdom
- ⁷⁸ Louisiana Tech University, Ruston LA, United States of America
- ⁷⁹ Laboratoire de Physique Nucléaire et de Hautes Energies, UPMC and Université Paris-Diderot and CNRS/IN2P3, Paris, France
- ⁸⁰ Fysiska institutionen, Lunds universitet, Lund, Sweden
- ⁸¹ Departamento de Física Teórica C-15, Universidad Autónoma de Madrid, Madrid, Spain
- ⁸² Institut für Physik, Universität Mainz, Mainz, Germany
- ⁸³ School of Physics and Astronomy, University of Manchester, Manchester, United Kingdom
- ⁸⁴ CPPM, Aix-Marseille Université and CNRS/IN2P3, Marseille, France

- ⁸⁵ Department of Physics, University of Massachusetts, Amherst MA, United States of America
- ⁸⁶ Department of Physics, McGill University, Montreal QC, Canada
- ⁸⁷ School of Physics, University of Melbourne, Victoria, Australia
- ⁸⁸ Department of Physics, The University of Michigan, Ann Arbor MI, United States of America
- ⁸⁹ Department of Physics and Astronomy, Michigan State University, East Lansing MI, United States of America
- ⁹⁰ (a) INFN Sezione di Milano; (b) Dipartimento di Fisica, Università di Milano, Milano, Italy
- ⁹¹ B.I. Stepanov Institute of Physics, National Academy of Sciences of Belarus, Minsk, Republic of Belarus
- ⁹² National Scientific and Educational Centre for Particle and High Energy Physics, Minsk, Republic of Belarus
- ⁹³ Department of Physics, Massachusetts Institute of Technology, Cambridge MA, United States of America
- ⁹⁴ Group of Particle Physics, University of Montreal, Montreal QC, Canada
- ⁹⁵ P.N. Lebedev Institute of Physics, Academy of Sciences, Moscow, Russia
- ⁹⁶ Institute for Theoretical and Experimental Physics (ITEP), Moscow, Russia
- ⁹⁷ Moscow Engineering and Physics Institute (MEPhI), Moscow, Russia
- ⁹⁸ D.V.Skobel'syn Institute of Nuclear Physics, M.V.Lomonosov Moscow State University, Moscow, Russia
- ⁹⁹ Fakultät für Physik, Ludwig-Maximilians-Universität München, München, Germany
- ¹⁰⁰ Max-Planck-Institut für Physik (Werner-Heisenberg-Institut), München, Germany
- ¹⁰¹ Nagasaki Institute of Applied Science, Nagasaki, Japan
- ¹⁰² Graduate School of Science and Kobayashi-Maskawa Institute, Nagoya University, Nagoya, Japan
- ¹⁰³ (a) INFN Sezione di Napoli; (b) Dipartimento di Fisica, Università di Napoli, Napoli, Italy
- ¹⁰⁴ Department of Physics and Astronomy, University of New Mexico, Albuquerque NM, United States of America
- ¹⁰⁵ Institute for Mathematics, Astrophysics and Particle Physics, Radboud University Nijmegen/Nikhef, Nijmegen, Netherlands
- ¹⁰⁶ Nikhef National Institute for Subatomic Physics and University of Amsterdam, Amsterdam, Netherlands
- ¹⁰⁷ Department of Physics, Northern Illinois University, DeKalb IL, United States of America
- ¹⁰⁸ Budker Institute of Nuclear Physics, SB RAS, Novosibirsk, Russia
- ¹⁰⁹ Department of Physics, New York University, New York NY, United States of America
- ¹¹⁰ Ohio State University, Columbus OH, United States of America
- ¹¹¹ Faculty of Science, Okayama University, Okayama, Japan
- ¹¹² Homer L. Dodge Department of Physics and Astronomy, University of Oklahoma, Norman OK, United States of America
- ¹¹³ Department of Physics, Oklahoma State University, Stillwater OK, United States of America
- ¹¹⁴ Palacký University, RCPTM, Olomouc, Czech Republic
- ¹¹⁵ Center for High Energy Physics, University of Oregon, Eugene OR, United States of America
- ¹¹⁶ LAL, Université Paris-Sud and CNRS/IN2P3, Orsay, France
- ¹¹⁷ Graduate School of Science, Osaka University, Osaka, Japan
- ¹¹⁸ Department of Physics, University of Oslo, Oslo, Norway
- ¹¹⁹ Department of Physics, Oxford University, Oxford, United Kingdom
- ¹²⁰ (a) INFN Sezione di Pavia; (b) Dipartimento di Fisica, Università di Pavia, Pavia, Italy
- ¹²¹ Department of Physics, University of Pennsylvania, Philadelphia PA, United States of America
- ¹²² Petersburg Nuclear Physics Institute, Gatchina, Russia
- ¹²³ (a) INFN Sezione di Pisa; (b) Dipartimento di Fisica E. Fermi, Università di Pisa, Pisa, Italy
- ¹²⁴ Department of Physics and Astronomy, University of Pittsburgh, Pittsburgh PA, United States of America
- ¹²⁵ (a) Laboratório de Instrumentação e Física Experimental de Partículas - LIP, Lisboa; (b) Faculdade de Ciências, Universidade de Lisboa, Lisboa; (c) Department of Physics, University of Coimbra, Coimbra; (d) Centro de Física Nuclear da Universidade de Lisboa, Lisboa; (e) Departamento de Física, Universidade do Minho, Braga; (f) Departamento de Física Teórica y del Cosmos and CAFPE, Universidad de Granada, Granada (Spain); (g) Dep Física and CEFITEC of Faculdade de Ciências e Tecnologia, Universidade Nova de Lisboa, Caparica, Portugal
- ¹²⁶ Institute of Physics, Academy of Sciences of the Czech Republic, Praha, Czech Republic
- ¹²⁷ Czech Technical University in Prague, Praha, Czech Republic
- ¹²⁸ Faculty of Mathematics and Physics, Charles University in Prague, Praha, Czech Republic
- ¹²⁹ State Research Center Institute for High Energy Physics, Protvino, Russia
- ¹³⁰ Particle Physics Department, Rutherford Appleton Laboratory, Didcot, United Kingdom
- ¹³¹ Physics Department, University of Regina, Regina SK, Canada
- ¹³² Ritsumeikan University, Kusatsu, Shiga, Japan
- ¹³³ (a) INFN Sezione di Roma; (b) Dipartimento di Fisica, Sapienza Università di Roma, Roma, Italy

- ¹³⁴ (a) INFN Sezione di Roma Tor Vergata; (b) Dipartimento di Fisica, Università di Roma Tor Vergata, Roma, Italy
- ¹³⁵ (a) INFN Sezione di Roma Tre; (b) Dipartimento di Matematica e Fisica, Università Roma Tre, Roma, Italy
- ¹³⁶ (a) Faculté des Sciences Ain Chock, Réseau Universitaire de Physique des Hautes Energies - Université Hassan II, Casablanca; (b) Centre National de l'Energie des Sciences Techniques Nucleaires, Rabat; (c) Faculté des Sciences Semlalia, Université Cadi Ayyad, LPHEA-Marrakech; (d) Faculté des Sciences, Université Mohamed Premier and LPTPM, Oujda; (e) Faculté des sciences, Université Mohammed V-Agdal, Rabat, Morocco
- ¹³⁷ DSM/IRFU (Institut de Recherches sur les Lois Fondamentales de l'Univers), CEA Saclay (Commissariat à l'Energie Atomique et aux Energies Alternatives), Gif-sur-Yvette, France
- ¹³⁸ Santa Cruz Institute for Particle Physics, University of California Santa Cruz, Santa Cruz CA, United States of America
- ¹³⁹ Department of Physics, University of Washington, Seattle WA, United States of America
- ¹⁴⁰ Department of Physics and Astronomy, University of Sheffield, Sheffield, United Kingdom
- ¹⁴¹ Department of Physics, Shinshu University, Nagano, Japan
- ¹⁴² Fachbereich Physik, Universität Siegen, Siegen, Germany
- ¹⁴³ Department of Physics, Simon Fraser University, Burnaby BC, Canada
- ¹⁴⁴ SLAC National Accelerator Laboratory, Stanford CA, United States of America
- ¹⁴⁵ (a) Faculty of Mathematics, Physics & Informatics, Comenius University, Bratislava; (b) Department of Subnuclear Physics, Institute of Experimental Physics of the Slovak Academy of Sciences, Kosice, Slovak Republic
- ¹⁴⁶ (a) Department of Physics, University of Cape Town, Cape Town; (b) Department of Physics, University of Johannesburg, Johannesburg; (c) School of Physics, University of the Witwatersrand, Johannesburg, South Africa
- ¹⁴⁷ (a) Department of Physics, Stockholm University; (b) The Oskar Klein Centre, Stockholm, Sweden
- ¹⁴⁸ Physics Department, Royal Institute of Technology, Stockholm, Sweden
- ¹⁴⁹ Departments of Physics & Astronomy and Chemistry, Stony Brook University, Stony Brook NY, United States of America
- ¹⁵⁰ Department of Physics and Astronomy, University of Sussex, Brighton, United Kingdom
- ¹⁵¹ School of Physics, University of Sydney, Sydney, Australia
- ¹⁵² Institute of Physics, Academia Sinica, Taipei, Taiwan
- ¹⁵³ Department of Physics, Technion: Israel Institute of Technology, Haifa, Israel
- ¹⁵⁴ Raymond and Beverly Sackler School of Physics and Astronomy, Tel Aviv University, Tel Aviv, Israel
- ¹⁵⁵ Department of Physics, Aristotle University of Thessaloniki, Thessaloniki, Greece
- ¹⁵⁶ International Center for Elementary Particle Physics and Department of Physics, The University of Tokyo, Tokyo, Japan
- ¹⁵⁷ Graduate School of Science and Technology, Tokyo Metropolitan University, Tokyo, Japan
- ¹⁵⁸ Department of Physics, Tokyo Institute of Technology, Tokyo, Japan
- ¹⁵⁹ Department of Physics, University of Toronto, Toronto ON, Canada
- ¹⁶⁰ (a) TRIUMF, Vancouver BC; (b) Department of Physics and Astronomy, York University, Toronto ON, Canada
- ¹⁶¹ Faculty of Pure and Applied Sciences, University of Tsukuba, Tsukuba, Japan
- ¹⁶² Department of Physics and Astronomy, Tufts University, Medford MA, United States of America
- ¹⁶³ Centro de Investigaciones, Universidad Antonio Narino, Bogota, Colombia
- ¹⁶⁴ Department of Physics and Astronomy, University of California Irvine, Irvine CA, United States of America
- ¹⁶⁵ (a) INFN Gruppo Collegato di Udine, Sezione di Trieste, Udine; (b) ICTP, Trieste; (c) Dipartimento di Chimica, Fisica e Ambiente, Università di Udine, Udine, Italy
- ¹⁶⁶ Department of Physics, University of Illinois, Urbana IL, United States of America
- ¹⁶⁷ Department of Physics and Astronomy, University of Uppsala, Uppsala, Sweden
- ¹⁶⁸ Instituto de Física Corpuscular (IFIC) and Departamento de Física Atómica, Molecular y Nuclear and Departamento de Ingeniería Electrónica and Instituto de Microelectrónica de Barcelona (IMB-CNM), University of Valencia and CSIC, Valencia, Spain
- ¹⁶⁹ Department of Physics, University of British Columbia, Vancouver BC, Canada
- ¹⁷⁰ Department of Physics and Astronomy, University of Victoria, Victoria BC, Canada
- ¹⁷¹ Department of Physics, University of Warwick, Coventry, United Kingdom
- ¹⁷² Waseda University, Tokyo, Japan
- ¹⁷³ Department of Particle Physics, The Weizmann Institute of Science, Rehovot, Israel
- ¹⁷⁴ Department of Physics, University of Wisconsin, Madison WI, United States of America
- ¹⁷⁵ Fakultät für Physik und Astronomie, Julius-Maximilians-Universität, Würzburg, Germany
- ¹⁷⁶ Fachbereich C Physik, Bergische Universität Wuppertal, Wuppertal, Germany

